
Civil Engineering Theses

Civil Engineering

Fall 4-16-2019

SEISMIC PERFORMANCE OF EARTH SLOPES SUBJECTED TO EARTHQUAKE MAINSHOCK – AFTERSHOCK SEQUENCES

alisha khanal

Follow this and additional works at: https://scholarworks.uttyler.edu/ce_grad



Part of the [Civil Engineering Commons](#), [Geotechnical Engineering Commons](#), and the [Risk Analysis Commons](#)

Recommended Citation

khanal, alisha, "SEISMIC PERFORMANCE OF EARTH SLOPES SUBJECTED TO EARTHQUAKE MAINSHOCK – AFTERSHOCK SEQUENCES" (2019). *Civil Engineering Theses*. Paper 10.

<http://hdl.handle.net/10950/1303>

This Thesis is brought to you for free and open access by the Civil Engineering at Scholar Works at UT Tyler. It has been accepted for inclusion in Civil Engineering Theses by an authorized administrator of Scholar Works at UT Tyler. For more information, please contact tgullings@uttyler.edu.

SEISMIC PERFORMANCE OF EARTH SLOPES SUBJECTED TO EARTHQUAKE
MAINSHOCK – AFTERSHOCK SEQUENCES

by

ALISHA KHANAL

A thesis submitted in partial fulfillment
of the requirements for the degree of
Master of Science
Department of Civil Engineering

Gokhan Saygili, Ph.D., P.E., Committee Chair
College of Engineering

The University of Texas at Tyler
May 2019

The University of Texas at Tyler
Tyler, Texas


This is to certify that the master's Thesis of

ALISHA KHANAL

has been approved for the thesis requirement on
3/27/2019
for the Master's in Civil Engineering

Approvals:


Thesis Chair: Gokhan Saygili, Ph.D. P.E.


Member: Torey Nalbhone, Ph.D.


Member: Micheal Gangone, Ph.D.


Chair, Department of Civil Engineering


Dean, College of Engineering

© Copyright 2019 by Alisha Khanal
All rights reserved.

Dedication

To My Dad

Acknowledgements

Thank you all for your help. I'm especially grateful to Dr. Gokhan Saygili for continuously supporting me and guiding throughout this study. He supervised me with all his knowledge in this field and gave me his valuable time. He's a great professor, supervisor and enthusiastic researcher. Without him this study would not have been possible. He's not only my advisor but my mentor too. He's given me a lot of motivation and encouraged me to move forward. I would also like to express my gratitude to Dr. Torey Nalbone and Dr. Micheal Gangone for reading my thesis and providing their valuable comments. Their guidance and valuable insights have helped clear numerous doubts I have had. I thank entire civil engineering department and graduate school for being so supportive.

I would like to thank my parents, Late Madhav Prasad Khanal and Sarmila Khanal for encouraging me to achieve everything I am today. Without them I wouldn't be able to complete my education so far and become a person I'm today.

Table of Contents

List of Tables	iii
List of Figures	iv
Abstract	vi
Chapter One Introduction.....	1
General	1
Problem definition	2
Objective	2
Thesis Organization	3
Chapter Two Literature Review.....	4
Introduction	4
Mainshock – Aftershock overview	4
Seismic Performance assessment of structures subjected to aftershocks	8
Slope stability	10
Limit Equilibrium method	11
Sliding block method	14
Rigid Sliding block method	15
Dynamic Response analysis	17
Flexible Sliding block method	19
Coupled and decoupled sliding displacement calculations	20
Discussion	21
Chapter Three Research workflow and analyses	23
Research Approach	23
Mainshock – aftershock ground motion database	24
Research Workflow	32
Summary	32
Chapter Four Dynamic response and sliding displacement analyses	34
Introduction	34
Calculation of the seismic loading parameters	35
Verification of existing predictive models for dynamic response	38
Sliding Displacement Analyses	42
Aftershock record selection	47

Summary	48
Chapter Five Effects of Aftershocks	50
Introduction	50
Development of sliding displacement predictive models that incorporate aftershocks	50
Case Study	56
Summary	59
Chapter Six Conclusions and Discussions	60
Future Recommendations:	62
List of Symbols and Notations	63
References	64
Appendix A: Mainshocks	72
Appendix B: Aftershocks	76
Vita	80

List of Tables

Table 1: Percent increase in decoupled sliding displacements in aftershock.....	53
Table 2: Summary of the predicted ground motion parameters.....	56
Table 3: Sliding displacements calculated with and without aftershocks for different site conditions for a slope with a $k_y=0.1$ g.....	57

List of Figures

Figure 1: M7.8 and M7.3 Nepal of April 2015 and May 2015 respectively	5
Figure 2: M8.6 and M8.2 Northern Sumatra, Indonesia Earthquakes of 11 April 2012 ...	6
Figure 3: M7.5 and M7.1 China, Tangshan Earthquakes of 28 July 1976	6
Figure 4: Map of central part of New Zealand's South Island depicting the intensity of shaking caused by the mainshock of Sept. 4, 2010, and the largest aftershock of Feb. 22, 2011	7
Figure 5: Rigid sliding block with the acceleration-time history, sliding velocity-time history and sliding displacement-time history	15
Figure 6: Seismic loading parameters for flexible sliding mass	20
Figure 7: Illustration of the research workflow	23
Figure 8: Earthquake magnitude distribution with respect to closest distance for selected (a) mainshocks and (b) aftershocks	26
Figure 9: Acceleration and velocity time histories for a strong motion record	28
Figure 10: (a) Development of Arias Intensity over time (b) evaluation of significant durations (D_{5-95} and D_{5-75}) from the normalized Arias Intensity	29
Figure 11: Distribution of Ground Motion Parameters PGA, PGV, Arias Intensity, T_m , D_{5-95} , D_{5-75} for selected mainshocks.	30
Figure 12: Distribution of Ground Motion Parameters PGA, PGV, Arias Intensity, T_m , D_{5-95} , D_{5-75} for selected aftershocks.	31

Figure 13: (a)Acceleration-time history and (b) Velocity-time history for ARE000.	36
Figure 14: The k-time history and k-vel – time history of site A for ARE000 motion ...	37
Figure 15: Distribution of (a) k_{\max} versus corresponding PGA and (b) $k\text{-vel}_{\max}$ versus corresponding to PGV	39
Figure 16: Variation of (a) k_{\max}/PGA and (b) $k\text{-vel}_{\max}/\text{PGV}$ versus T_s/T_m	41
Figure 17: Displacement residuals (a) scalar model and (b) vector model versus T_s/T_m	45
Figure 18: Displacement residuals versus the site period for (a) k_{\max} , M model and (b) k_{\max} , $k\text{-vel}_{\max}$ model	46
Figure 19 : Artificial aftershock displacement versus Recorded aftershock displacement	48
Figure 20: Predicted (a) k_{\max} , (b) $k\text{-vel}_{\max}$, and (c) sliding displacements as a function of the natural period of the sliding mass for a $M=7$, $R=5$ km event	52
Figure 21: Decoupled sliding displacement increase due to aftershocks	53
Figure 22: Decoupled Sliding displacements subjected to mainshock only and mainshock-aftershock sequence	55
Figure 23: Sliding displacement predictions for mainshock only and mainshock- aftershock sequence as a function of earthquake magnitude using the (a) k_{\max} , M model and (b) k_{\max} , $k\text{-vel}_{\max}$ model (Site B)	58

Abstract

SEISMIC PERFORMANCE OF EARTH SLOPES SUBJECTED TO EARTHQUAKE MAINSHOCK-AFTERSHOCK SEQUENCES

Alisha Khanal

Thesis Chair: Gokhan Saygili, Ph.D.

The University of Texas at Tyler
May 2019

Mainshocks are usually followed by aftershocks. Aftershocks continue over a period of time with a decreasing frequency and there is not sufficient time for repair and retrofit between a mainshock – aftershock sequence. Typically, aftershocks are smaller in magnitude; however, aftershock ground motion characteristics such as the intensity and duration can be greater than the mainshock due to the changes in the earthquake mechanism and location with respect to the site. The seismic performance of slopes is typically evaluated based on the sliding displacement predicted to occur along a critical sliding surface. Various empirical models are available that predict sliding displacement as a function of seismic loading, ground motion, and site parameters but these models do not include the aftershocks. Seismic risks associated with the post-mainshock slopes (“Damaged slopes”) subjected to aftershocks are significant. This study extends the empirical sliding displacement models for flexible slopes subjected to earthquake mainshock – aftershock sequences (a multi hazard approach). A comprehensive dataset was developed using 144 pairs of as-recorded mainshock – aftershock sequences using

Pacific Earthquake Engineering Research (PEER) database. The predictive models are functions of seismic loading, ground motion, site, and slope parameters. The results revealed that decoupled sliding displacements of post-mainshock slopes subjected to aftershocks increased on average around 30% at all site periods due to the combined effects of strength degradation and additional seismic demand by the aftershock. A case study is demonstrated to explain the effects of aftershocks on the seismic performance of post-mainshock flexible sliding masses. Overall, the results suggest that aftershocks increase the seismic demand relative to the mainshock alone; thus, the seismic risk is underestimated if aftershocks are neglected.

Chapter One

Introduction

General

An earthquake is a sudden and violent shaking of the ground. The most common causes are the movement of tectonic plates beneath Earth's crust, volcanic action, and human activities such as hydraulic fracturing and deep injection. Depending upon the intensity and duration characteristics, earthquakes can have devastating effects on both human lives and the infrastructure. Generally, an earthquake is not a stand-alone event. Any single earthquake event is usually preceded and followed by a number of events of smaller magnitude (or sometimes greater magnitude). Earthquakes in a sequence are broadly differentiated into foreshocks, mainshock, and aftershocks. The U.S Geological Survey (USGS) defines the mainshock as the largest earthquake in a sequence, sometimes preceded by one or more foreshocks, and almost always followed by many aftershocks. Aftershocks are usually smaller than the mainshock and can continue over a period of weeks, months, or even years. In general, the larger the mainshock, the larger and more numerous the aftershocks. However, in some cases it was documented that the magnitude or shaking intensity of aftershocks exceed those of mainshocks.

The earthquakes caused by human activities such as mining and fracking are categorized as induced seismicity. These earthquakes typically have relatively small magnitudes, but some moderate man-made earthquakes have recently occurred. For example, the 1952 El Reno earthquake of 5.7 magnitude was caused due to the deep injection of waste water (Hough and Page 2015). Induced seismicity can also be caused

due to injection of carbon dioxide as a storage step for carbon capture and storage. The induced seismicity is out of the scope of this research.

Problem definition

Earthquakes can trigger landslides that can significantly damage the infrastructure. An earthquake-induced landslide is defined as the downward or upward movement of slope forming materials due to seismic activity. There have been numerous studies focusing on the behavior of slopes during an earthquake. However, the vast majority of these studies consider earthquake as a single event, i.e., they do not account for the entire mainshock – aftershock sequence. To date, the occurrence of aftershocks (i.e., multi-hazard approach) has not been included in the assessment of seismic performance of earth slopes. In the geotechnical earthquake engineering literature, there is a knowledge gap regarding the evaluation of the seismic performance of earth slopes subjected to multiple earthquakes (i.e., mainshock – aftershock sequences).

Objective

The combination of a mainshock and aftershock increases the seismic demand on slopes relative to the mainshock alone; thus, seismic risks may be underestimated if aftershocks are neglected. The main objective of this research is to provide an improved assessment of risks associated with the seismic performance of earth slopes subjected to earthquake mainshock-aftershock sequences. The research plan has the following objectives:

- 1:** Investigate the effects of aftershock selection to represent mainshock – aftershock sequences by studying commonly followed approaches (e.g, repeated seismic sequence, randomized seismic sequence, and as-recorded seismic sequence)

2: Investigate the effects of aftershocks on the seismic performance of post-mainshock slopes

3: Investigate the impacts of strength degradation on the yield acceleration of post-mainshock slopes subjected to aftershocks

4: Investigate and develop sliding displacement predictive models that incorporate the effects of aftershocks. These models will predict the sliding displacement as a function of ground motion parameters and site parameters.

Thesis Organization

Chapter 1 presents a brief discussion about the research objectives and thesis organization.

Chapter 2 presents a number of case histories subjected to mainshock – aftershock sequences. It also presents a brief overview of the common procedures used by researchers and practicing engineers to evaluate the performance of rigid and flexible slopes under earthquake loading conditions.

Chapter 3 describes the strong motion database and research workflow followed to perform dynamic response and sliding displacement analyses at various site and slope conditions.

Chapter 4 presents the results of the dynamic response and sliding displacement analyses performed throughout this research. It also describes the procedure followed for the selection of aftershock records.

Chapter 5 presents effects of aftershocks on post-mainshock “damaged” slopes. A case study is demonstrated to explain the effects of aftershocks on the seismic performance of post-mainshock flexible sliding masses

Chapter 6 includes the conclusions from this study and discussions of the work done.

Chapter Two

Literature Review

Introduction

Medium to large earthquakes with magnitudes measuring 4 to 7 on the Richter scale can trigger landslides. Earthquake-induced landslides can cause significant damage to the critical infrastructure and community. Typically, aftershocks are followed by the mainshock and they continue over a period of time with a decreasing frequency and there is not sufficient time for repair and retrofit between mainshock – aftershock sequences. Following the mainshock, aftershocks may further contribute to additional damage on geo-structures (e.g. earth slopes). It is therefore necessary to account for aftershocks in the performance assessment of earth slopes under earthquake loading conditions.

Mainshock – Aftershock overview

Typically, aftershocks are smaller in magnitude; however, aftershock ground motion characteristics such as the intensity and duration can be greater than that of the mainshock due to the changes in the earthquake mechanism and location with respect to the site (Figures 1 to 4). Thus, aftershocks can cause as much (or in some cases even more severe) damage as the mainshock. In what follows, four case histories are briefly presented to demonstrate mainshock – aftershock sequences.

A 7.8 magnitude earthquake hit Barpak, Gorkha of Nepal on April 25, 2015. This earthquake was followed by more than 20,000 aftershocks out of which there was a major aftershock of 7.3 magnitude on Sindhupalchowk district on May 12, 2015 as shown in Figure 1. The red dots represent the epicenters of the aftershocks. In this case,

there was more destruction due to the aftershock on the May 12, 2015 than the mainshock.

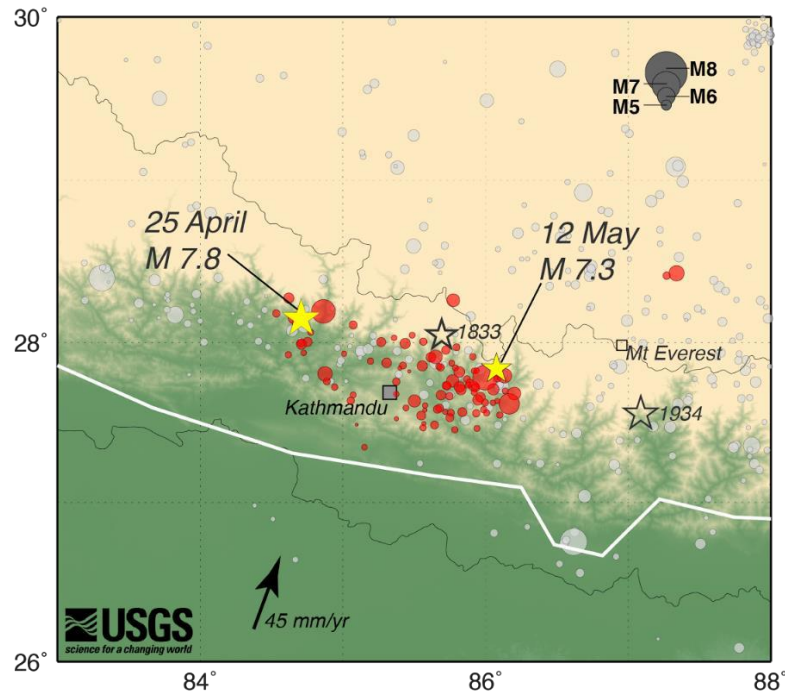


Figure 1: M7.8 and M7.3 Nepal of April 2015 and May 2015 respectively
(USGS 2015)

The 2012 M8.6 mainshock off the West Coast of Northern Sumatra in Indonesia was followed by several strong aftershocks in just over two hours (USGS 2012). The region experienced severe post-mainshock shaking due to strong aftershocks. Figure 2 shows the epicenters of the mainshock and aftershocks, with the largest measured at M8.2.

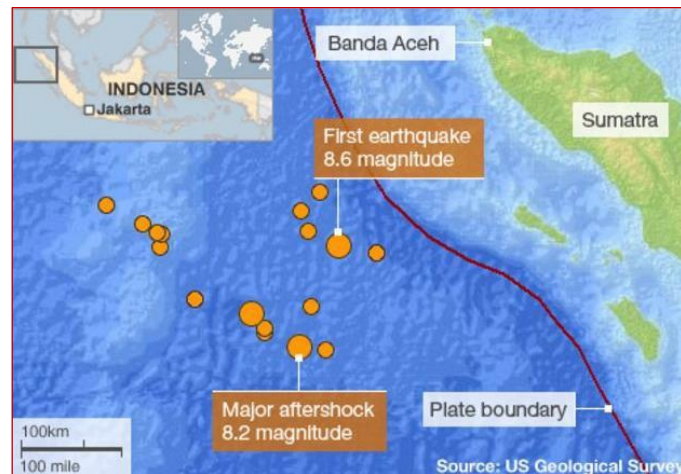


Figure 2: M8.6 and M8.2 Northern Sumatra, Indonesia Earthquakes of April 11, 2012 (USGS 2012)

A M7.5 earthquake struck Tangshan city of China in 1976. Numerous aftershocks occurred following the mainshock. The largest aftershock that was measured at M7.1 occurred in the same day in Luanxian city. Figure 3 shows the epicenters of the mainshock and the major aftershock. Again, the major aftershock was as strong as the mainshock.

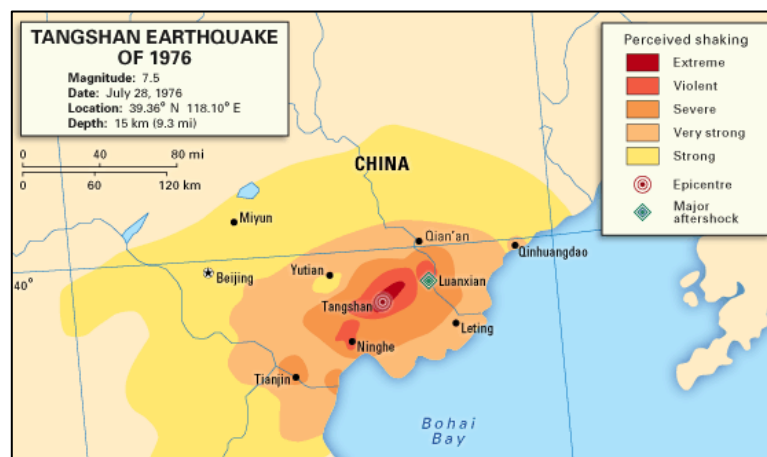


Figure 3: M7.5 and M7.1 China, Tangshan Earthquakes of July 28, 1976 (Encyclopaedia Britannica 2018)

A series of mainshock–aftershock sequences struck New Zealand during 2010 and 2011. The M7.1 mainshock occurred in the vicinity of the city of Darfield on September 4, 2010 and was followed by several severe aftershocks (Figure 4). The largest aftershock occurred on February 22, 2011 (M_w 6.2 Christchurch earthquake) but there was not sufficient time for repair and retrofit between mainshock – aftershock sequences. The depth of the mainshock was estimated to be 10 km whereas the depth of the largest aftershock was estimated to be 5 km.

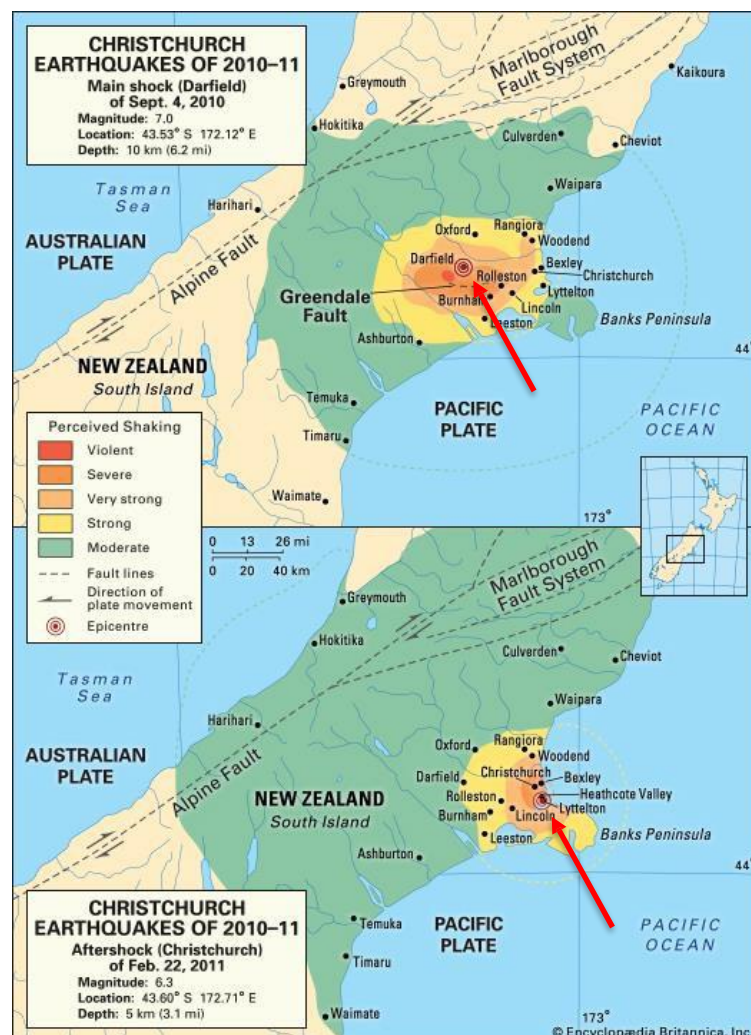


Figure 4: Map of central part of New Zealand's South Island depicting the intensity of shaking caused by the mainshock of Sept. 4, 2010, and the largest aftershock of Feb. 22, 2011 (Encyclopaedia Britannica 2017)

These case histories are good examples to show that aftershocks can generate significant ground motion hazard. In essence, seismic risks associated with the post-mainshock slopes (“Damaged slopes”) subjected to aftershocks is significant. Recently, the seismic performance and collapse vulnerability considering mainshock – aftershock sequences has been studied for reinforced concrete frame buildings [Raghunandan et al. (2015); Jeon et al. (2015); Han et al. (2014)], wood frame structures [Goda (2014); Yin and Li (2010)], and steel frame buildings [Ruiz-Garcia and Aguilar (2017); Li et al. (2014); Song et al. (2014); Ruiz-García and Negrete-Manriquez (2011)]. To date, the occurrence of aftershocks (i.e., multi-hazard approach) has not been included in the assessment of seismic performance of earth slopes. In the geotechnical earthquake engineering literature, there is a knowledge gap regarding the evaluation of the seismic performance of earth slopes subjected to mainshock – aftershock sequences. The next section presents a brief overview of the current research studies on the seismic performance of structures subjected to mainshock-aftershock sequences.

Seismic Performance assessment of structures subjected to aftershocks

Raghunandan et al. (2015) studied the aftershock collapse vulnerability assessment of reinforced concrete frame structures. If the building is not severely damaged in the mainshock, its collapse capacity is unaffected in the aftershock. However, if the building is extensively damaged in the mainshock, there is a significant reduction in its collapse capacity in the aftershock. In general, the occurrence rate of aftershocks decreases as time goes by after the mainshock. The magnitude of an aftershock is usually less than mainshock, but the aftershock may have a higher intensity and longer duration than the mainshock. The combination of a mainshock –

aftershock sequence would require the structures to dissipate more energy (Li, Song and Van De Lindt 2014).

Song et al. (2014) documented that both the duration and frequency content of ground motion plays important role in structural collapse capacity of structures. The extent of the structural damage after the mainshock can also influence the effect of the aftershocks on the structures. Therefore, post-mainshock structures with severe damage states maybe be more fragile when subjected to aftershocks with longer duration and lower frequency.

Many of the studies that provide information on the effects of seismic sequences on the response of structures employ artificial seismic sequences instead of as-recorded mainshock-aftershock sequences. The two major approaches used for generating these artificial sequences are the back-to-back (repeating) approach and randomizing the set of mainshock acceleration time-history to simulate the following aftershocks. The back-to-back application of mainshock records as aftershock is often considered by conducting aftershock incremental dynamic analysis. In such an approach, the characteristics of mainshock records are considered to be similar to those of major aftershock records within the same mainshock–aftershock sequences. The underlying assumption is that the characteristics of selected mainshocks, other than those used for record selection, are not significant in the assessment of structural responses Goda (2014). Goda (2014) studied how the selected aftershock ground motion records, when scaled up, affect the evaluation of non-linear response potential due to mainshock - aftershock sequences. They observed that the response caused by the scaled mainshock and aftershock records may differ significantly compared to the results obtained using as-recorded aftershocks. Therefore, they concluded that it is desirable to use ground

motion input that best represents the actual seismic environment under consideration. According to Ruiz-García and Negrete-Manriquez (2011) the use of scaled mainshock approach is the 'worst' seismic scenario which might be unlikely to occur in earthquake-prone regions. Ruiz-García and Negrete-Manriquez (2011) also observed that the mainshock and the main aftershock have very different predominant periods of ground motions and, therefore, very different frequency content. They reported that the frequency content of mainshock and main-aftershock ground motion is weakly correlated from a statistical point-of-view which leads to the conclusion that the simulation approach of repeating the mainshock as an aftershock is not appropriate.

Slope stability

This section presents a brief overview of the common procedures used by researchers and practicing engineers to evaluate the performance of slopes under earthquake loading conditions. Earth slopes naturally exist in states ranging from 'very stable' to 'marginally' stable. In this context, a slope is labelled as marginally stable if the factor of safety is close to unity in its natural state. Often times, ground shaking is sufficient to cause damage in 'marginally' to 'moderately' stable slopes. The resulting damage depends upon the shaking severity as well as the geometric and materials characteristics of the slope. In his Geotechnical Earthquake Engineering textbook, Kramer (1996) reports that 56% of the total cost of damage following the 1964 Alaska earthquake was attributed to earthquake-induced landslides. In Japan, of the casualties due to earthquakes over M6.9 between 1964 to 1980, more than half were caused by landslides. Furthermore, hundreds of landslides were caused due to the 1920 Haiyuan earthquake (M=8.5) in China which resulted in over a hundred thousand deaths. Recently, the 2008 Greece Earthquake at Achaia-Ilia caused a number of landslides and

rockfalls over a wide area with the most distant ones occurring approximately 100 km from the epicenter (Margaris et al., 2008). More recently, the 2015 M7.8 Earthquake in Nepal induced landslides over a broad area that led to significant flood risks (Hashash et al., 2015). The M6.3 Meinong Earthquake of 2016 caused several large slope failures with four failures along the Tsengwen river out of which two occurred in areas protected by concrete facing and two along graded slopes (Sun et al., 2016). Therefore, the evaluation of seismic slope stability is of major concern for geotechnical earthquake engineering (Kramer 1996).

Limit Equilibrium method

Traditionally, the limit equilibrium method has been used for the stability analysis of slopes. This approach considers the shear stresses along a failure surface and computes factor of safety based on the available shear strength and the shear stresses required for equilibrium. The factor of safety for these methods can be defined as the ratio of shear strength of soil to shear stress required for equilibrium. The minimum factor of safety for a slope is estimated by trial and error for a large number of assumed slip surfaces.

The so-called method of slices divides the potential slip surface into a number of slices. It is commonly used for the stability analysis of slopes as they can solve for complex geometries as well as varying soil and water pressure conditions. In a slope stability problem, the number of equations of equilibrium available is smaller than the number of unknowns. Therefore, equilibrium methods employ certain assumptions to make the problem determinate. However, the factor of safety obtained by these methods

is only as reliable as the data and assumptions made. For instance, the force equilibrium methods [e.g. Lowe et al. (1960); US Army Corps of Engineers (1968)] satisfy both horizontal and vertical force equilibrium but they do not satisfy the moment equilibrium. In force equilibrium methods, the factor of safety is affected significantly by assumed inclinations of the side forces between the slices whereas for methods that satisfy all conditions for equilibrium, e.g. Janbu's (1954) Generalized Procedure of Slice and Morgenstern Price's Method (1965) the influence of the assumptions on the value of the factor of safety is insignificant (Duncan 1996).

Fredlund and Krahn (1977) made a comparison of different methods for slope stability analysis. The ordinary method of slices, considered as the simplest method, provides a linear factor of safety equation. However, it fails to satisfy Newton's third law of motion between slices and this causes errors in results during the factor of safety calculation of which can be as high as 60% (Whitman and Bailey 1967). The simplified Bishop method (1955) neglects the interslice shear forces and assumes that the horizontal (normal) force sufficiently defines the interslice forces. Spencer's method (1967) assumes there is a constant relationship between magnitude of interslice shear and normal forces. Spencer (1967) derived two factor of safety equations: from summation of moments about a point & from summation of forces about a point. Thus, both moment and force equilibrium are satisfied. Janbu's (1954) simplified method uses correction factor f_0 to account for effect of interslice shear forces. The factor of safety is obtained by multiplying f_0 with the factor of safety obtained through summation of horizontal and vertical forces while ignoring interslice shear forces. Janbu's (1954) rigorous method assumes that the point at which the interslice forces act can be defined by a 'line of thrust'. It differs from the simplified method in that the interslice shear

forces are included in the derivation of normal force and thus the factor safety. The Morgenstern-Price method assumes an arbitrary mathematical function to describe the direction of interslice forces. This method calculates factor of safety through summation of tangential and normal forces to each slice. It accounts for both force and moment equilibrium (Fredlund and Krahn 1977).

An implicit assumption in equilibrium analyses of slope stability is that the stress-strain behavior of the soil is ductile, i.e., the shear resistance of the soil does not drop drastically after reaching the peak in stress-strain curve (Duncan 1996). Therefore, the strains within the slopes or their variation along a slip surface are not considered in this approach (i.e., rigid body). As a result of this limitation, unless the stress-strain behavior is ductile, peak strength might not be mobilized simultaneously along the full slip surface. If the behavior is not ductile, i.e., the shearing resistance drops off abruptly after reaching the peak, progressive failure can occur and the shearing resistance that can be mobilized at some points may be smaller than the peak strength. In such cases, the reliable way to get around this problem is to use residual strength rather than peak strength in the analysis (Duncan 1996).

The limit equilibrium methods for analyzing the stability of slopes under seismic loading consist of dividing the failure surface into a number of sections (slices) and analyzing the stability of each slice using horizontal and vertical pseudostatic (seismic) coefficients to calculate horizontal and vertical forces during a potential earthquake. In that regard, a pseudostatic slope stability analysis is a limit equilibrium procedure that models earthquake shaking as a destabilizing horizontal ‘static’ force. This approach significantly simplifies the problem but is not an accurate representation of earthquake shaking. Newmark (1965) observed that with dynamically applied loads,

the force may act in one direction for only tenths of a second before it reverses its direction. Hence, the major limitation of this approach is that it defines the dynamic effects of an earthquake as a constant horizontal force acting in only one direction (J. D. Bray, Pseudostatic Coefficient for Use in Simplified Seismic Slope Stability Evaluation 2009). It has also been found that applying pseudostatic force in the horizontal direction without a vertical component is the most conservative assumption whereas, applying the pseudostatic force in the horizontal direction with a vertical component provides unconservative estimates (Saygili 2008).

Sliding block method

The pseudostatic approach provides a crude estimate of the seismic performance of slopes; however, it does not accurately represent the earthquake shaking. Sliding block methodology; however, acknowledges that the horizontal force induced by earthquake shaking is variable and that at some instances in time this force may result in factors of safety less than 1.0. Given the limitations of the pseudostatic analysis, the seismic performance of slopes and earth structures is often assessed by the sliding displacement predicted to occur along a critical sliding surface. This displacement represents the cumulative, downslope movement of a sliding mass due to earthquake shaking. The magnitude of sliding displacement relates well with observations of seismic performance of slopes e.g. Jibson et al. (2000), and thus has been a useful parameter in seismic design and hazard assessment.

Sliding block method has been observed to be useful to evaluate the performance of embankments made of clayey soils, moist or dry cohesionless soils, and dense cohesionless soils. Newmark (1965) realized that accelerations generated by

earthquake shaking could impart a destabilizing force sufficient to reduce temporarily the factor of safety of a slope below 1.0, leading to sliding episodes and the accumulation of permanent, downslope sliding displacement. The original Newmark procedure models the sliding mass as a rigid body and uses yield acceleration and acceleration-time history of rigid foundation beneath the sliding mass. However, this approach does not consider for the dynamic response of flexible slopes. In essence, the dynamic response has a minor impact on the sliding displacements of shallow soil masses (i.e. rigid slopes) because the natural period of a thin soil layer is negligible.

Rigid Sliding block method

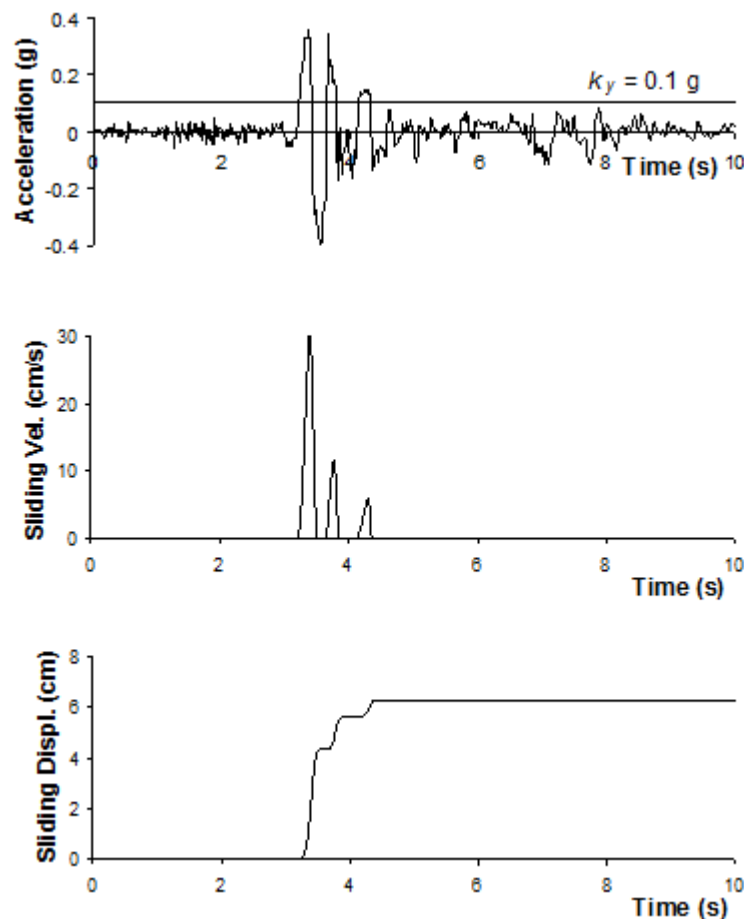


Figure 5: Rigid sliding block with the acceleration-time history, sliding velocity-time history and sliding displacement-time history (Saygili and Rathje 2008)

For natural slopes with potential for shallow failure, the rigid sliding block analysis is the most common analytical procedure used to predict the potential for earthquake-induced landslides. The slope is intact with the base (foundation) and when acceleration exceeds k_y , there's a sliding episode that continues until the velocity of the sliding block and foundation coincide. On integrating this velocity, we get a sliding displacement (Figure 5). In practice, the expected permanent displacement for a slope is often assessed by either (1) selecting a suite of earthquake ground motion appropriate for the design event, computing the sliding displacement for each motion using yield acceleration of the slope, and computing the median and standard deviation of the computed displacements, or (2) using design charts and equations that predict sliding displacement based on various ground motion parameters and the yield acceleration.

There have been various predictive models proposed that predict rigid block sliding displacement as a function of ground motion parameters like peak ground acceleration (PGA), Arias intensity, etc. [Franklin and Chang (1977); (Ambraseys and Menu (1988); Yegia et al. (1991); Ambraseys and Srbulov (1994)] developed charts and/or predictive equations for rigid sliding displacements using different ground motion data sets. However, because of the limited data sets, the resulting predictive equations displayed very large variability. Larger ground motion data sets have been used to develop similar predictive models in more recent research with better estimates of variability. Watson-Lamprey and Abrahamson (2006) developed a model for rigid block displacement using a large set consisting of 6,158 recording scaled with seven different scale factors and computed for three values of yield acceleration. This displacement model is a function of various parameters including PGA, spectral acceleration at a period of 1s ($Sa_{T=1s}$), root mean square acceleration (A_{rms}), k_y , and the

duration for which the acceleration-time history is greater than the yield acceleration (Dur_{ky}). However, a standard deviation for the predictive model was not presented, although this information was available for preliminary versions of the model and ranged from 0.3 to 0.7 in natural log space (Saygili and Rathje 2008).

Saygili and Rathje (2008) identified shallow sliding failure as the predominant failure mechanism in earthquake induced failure of natural slopes and a developed an empirical predictive model for rigid block sliding that predicts displacement as a function of multiple ground motion parameters. Based on their study, two parameter vector models of (PGA, PGV) and the three-parameter vector model of (PGA, PGV, I_a) were shown to significantly reduce $\sigma_{\ln D}$ for displacement prediction. The multi-parameter models were also found to be more sufficient in predicting displacements over a range of earthquake magnitudes. However, since these models ignore the dynamic response of the slopes, they could not account for the behavior of flexible slopes (i.e., behavior after the slope has yielded).

Dynamic Response analysis

The dynamic response of rigid sliding masses is negligible and can be ignored. However, the dynamic response must be taken into account on deeper and softer sliding masses (i.e. flexible sliding masses) for the estimation of seismic demand. This section provides a brief overview of the procedure to evaluate the dynamic response of flexible sliding masses.

According to Kramer (1996), for linear elastic, one dimensional wave propagation, the equivalent-linear analysis method assumes the soil to behave as a

Kelvin-Voigt solid where the dynamic response is described using a purely elastic spring and a purely viscous dashpot. The slope is assumed to slide downward with constant yield acceleration. The strength properties of the soil are assumed independent of ground shaking (Strenk 2010). The dynamic response analyses are performed in frequency domain which requires a Fourier transformation to switch to the frequency from time domain. The properties that govern the dynamic response of a system are mass, stiffness, and damping. For a soil body under dynamic loading, the mass of the system is characterized by the mass density (ρ) and the height of the layer (h) while the stiffness is characterized by shear modulus and the damping is characterized by viscous damping ratio. For simplicity, the non-linear soil response is assumed linear elastic. Here, strain compatible shear modulus (G) and damping ratio (D) values are iteratively calculated based on the computed strain. Defining the mass density of a system is a straightforward process and the values of density of a given soil type can be predicted with an acceptable degree of certainty. Similarly, the height of a soil layer is constant for a given site condition and does not cause problems. However, the characterization of stiffness (shear modulus, G) and damping properties (D) is more complicated and requires both field and laboratory tests to predict with certainty. Therefore, the nonlinear behavior of G and D are achieved through modulus reduction and damping curves that describe the variation of G/G_{\max} and D with shear strain where, G_{\max} is the small strain shear modulus calculated by in situ measurement of shear-wave velocity as a function of depth (Kottke and Rathje 2009).

One output of a dynamic response analyses is the shear stress along the base of the sliding mass. The average acceleration within the sliding mass (k) can be computed using the formula $k = \tau/\gamma H$, where τ is the shear stress along the base of the sliding

mass, γ is the unit weight of soil, and H is the depth of sliding mass. Here, k is units of acceleration due to gravity (g). A k -time history can be numerically integrated over time to generate the k -vel time history. The maximum values on the k -time history and k -vel time histories are called k_{\max} and $k\text{-vel}_{\max}$, respectively (Antonakos and Rathje, A unified model for predicting earthquake-induced sliding displacements of rigid and 2011).

Flexible Sliding block method

The seismic loading parameters (k_{\max} and $k\text{-vel}_{\max}$) are obtained from the dynamic response of the sliding mass. As illustrated in Figure 6, the seismic loading parameters are used to calculate the sliding displacements on flexible soil masses. When k values exceed the yield acceleration (k_y) of the sliding mass, sliding episodes initiate. Sliding continues until the velocity of the sliding block and foundation coincide. Antonakos and Rathje (2011) proposed empirical models to predict the seismic loading parameters. This study has been very pivotal in this study; therefore, the details of the predictive model are discussed in Section 4.3.

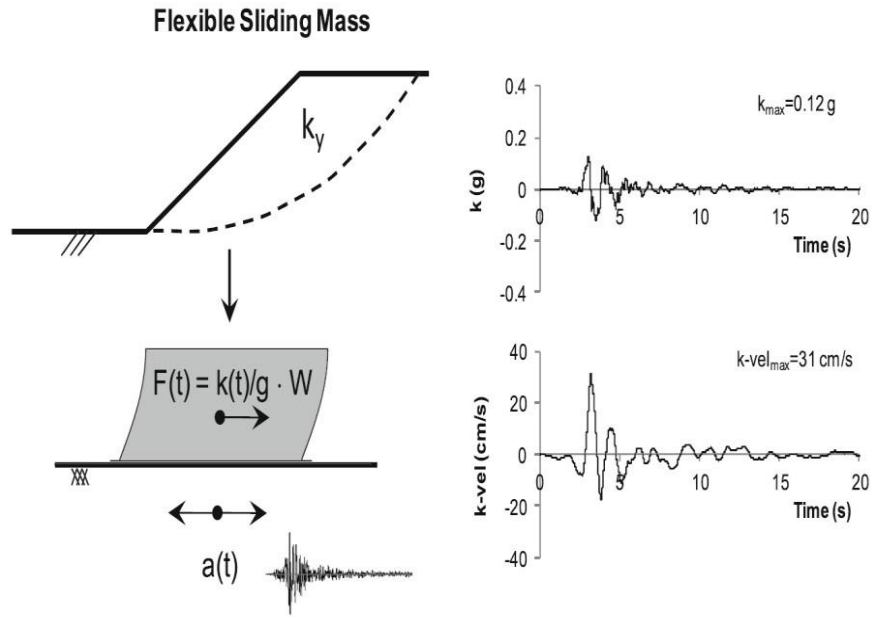


Figure 6: Seismic loading parameters for flexible sliding mass (Rathje, Wang, et al. 2014)

Coupled and decoupled sliding displacement calculations

For the sliding displacement calculations, two procedures have been followed. They are called the coupled and decoupled procedures. The decoupled technique consists of separate computation steps for the dynamic response and sliding calculations. The dynamic response analysis generates the time dependent acceleration (horizontal equivalent acceleration time history) of the flexible sliding mass. Sliding calculations are performed separately using the k -time history. The decoupled analysis assumes that the dynamic response analysis and sliding calculations are two distinct steps, with each step having its own sets of assumptions (Strenk 2010). Makdisi and

Seed (1978) simplified the decoupled analysis by producing design charts to predict the co-seismic displacements. The sliding block displacement methodology (decoupled sliding block analysis) has been extended to account for the deformable response of sliding masses and considers the dynamic response which causes varying acceleration within the sliding mass.

While the decoupled model is an improvement over the rigid-block model, its underlying assumption that the sliding response and dynamic response can be separated is not “realistic”. These two responses are actually interdependent and interactive. The coupled model simultaneously models both dynamic and sliding response and thus is a significant improvement over the two-step decoupled model (Strenk 2010). Bray and Travarasrou (2007) developed a nonlinear, fully coupled sliding block model which used a semi-empirical method to predict sliding displacement as a function of yield acceleration, fundamental period of sliding mass, and spectral acceleration.

The coupled model provides a more complete picture of the sliding mechanism and is more accurate than the decoupled procedure. However, decoupled models provide reasonable results; thus, they are commonly used to evaluate the seismic stability of engineered slopes (Saygili 2008). In this study, decoupled sliding displacements are calculated.

Discussion

To date, the occurrence of aftershocks (i.e., multi- hazard approach) has not been included in the assessment of seismic performance of earth slopes. In the geotechnical earthquake engineering literature, there is a knowledge gap regarding the evaluation of the seismic performance of earth slopes subjected multiple earthquakes (i.e. mainshock-aftershock sequences). This chapter presents a number of case histories to demonstrate

that aftershocks can generate significant ground motion hazard. Next, some of the recent research studies on the seismic performance of structures subjected to mainshock-aftershock sequences are presented. Finally, a brief overview of the common procedures used by researchers and practicing engineers to evaluate the performance of rigid and flexible slopes under earthquake loading conditions is presented.

Chapter Three

Research workflow and analyses

Research Approach

The main objective of this research is to improve the existing empirical sliding displacement models for flexible slopes subjected to earthquake mainshock-aftershock sequences. This objective requires that dynamic response and sliding displacement analyses are performed using a large and high-quality dataset for strong motion records. This chapter describes the developed strong motion database and research workflow followed to perform dynamic response and sliding displacement analyses. An illustration of the research workflow is shown in Figure 7.

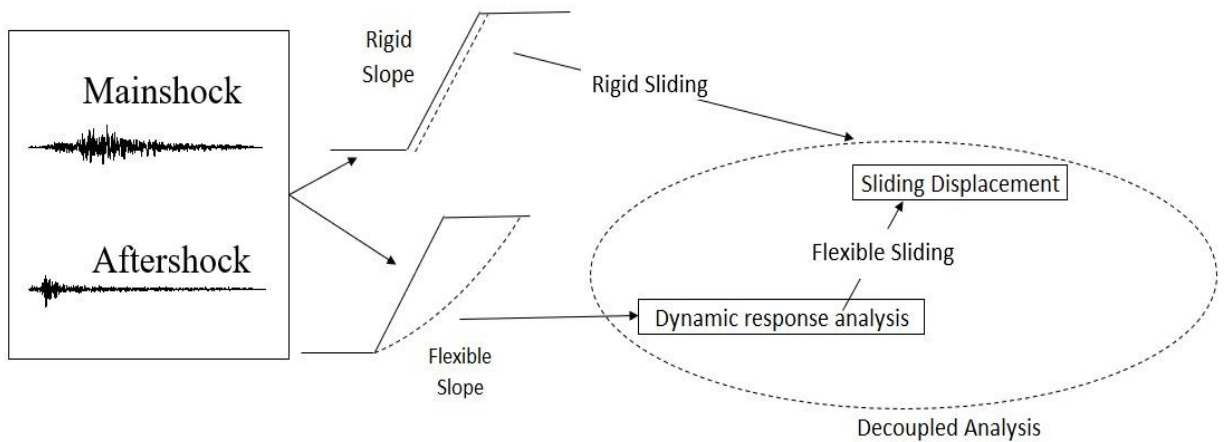


Figure 7: Illustration of the research workflow

For this study, 144 pairs of mainshock and aftershock strong ground motion pairs were taken from the PEER Database. Vrymoed and Calzascia (1978) and recently Rathje and Bray (2001) showed that dynamic response analyses using one-dimensional soil column provides an adequate estimate of the seismic loading in earth slopes. The k-time histories were obtained by approximating the dynamic response of a sliding mass

as a 1-D wave propagation problem. Next, k -vel – time histories were obtained by integrating the k – time histories over time. Finally, decoupled sliding displacements were computed using the k -time histories as input for various site and slope conditions. The maximum decoupled sliding displacements were taken into consideration for the development of the predictive models for flexible slopes subjected to mainshock and aftershock sequences.

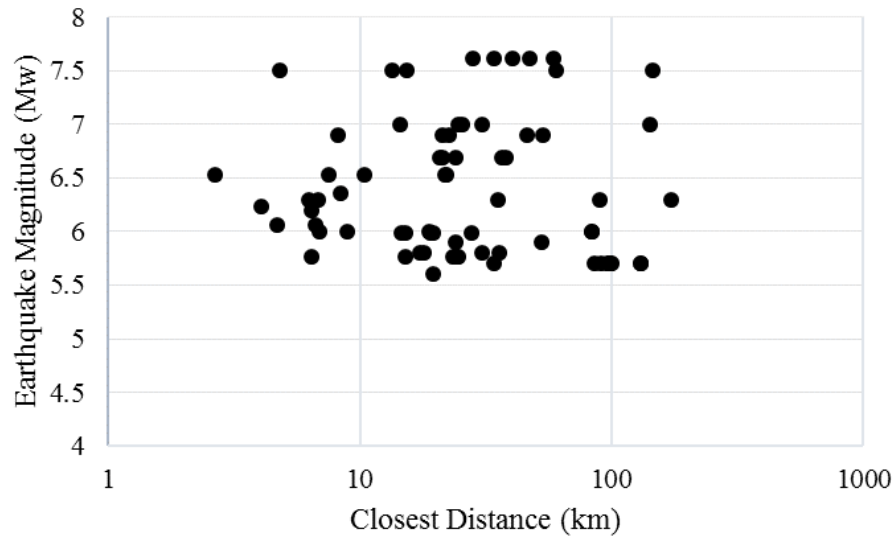
Mainshock – aftershock ground motion database

There are two common practices to represent the strong motion data for mainshock – aftershock sequences. These are the use of artificial time histories and as-recorded time histories. Artificial time histories are generated by scaling mainshock records as aftershocks. Here, the frequency content and duration characteristics are assumed to be the same. The variability in the intensity and characteristics of the ground motion is the most significant uncertainty in the prediction of the expected level of earthquake-induced sliding displacement. In essence, the ground motion characteristics of the mainshock and aftershocks can be remarkably different than each other. Typically, aftershocks are smaller in magnitude; however, aftershock ground motion characteristics such as the intensity and duration can be greater than the mainshock due to the changes in the earthquake mechanism and location with respect to the site (Song, Li and Van de Lindt 2014). For example, the duration of the aftershock ($M_w = 7.14$) recorded at station YPC150 following the Kocaeli, Turkey EQ in 1999 was two times longer than that of the mainshock ($M_w = 7.51$). Similarly, the magnitude and hence the intensity of ground motion parameters (e.g. PGA and PGV) recorded for the aftershock

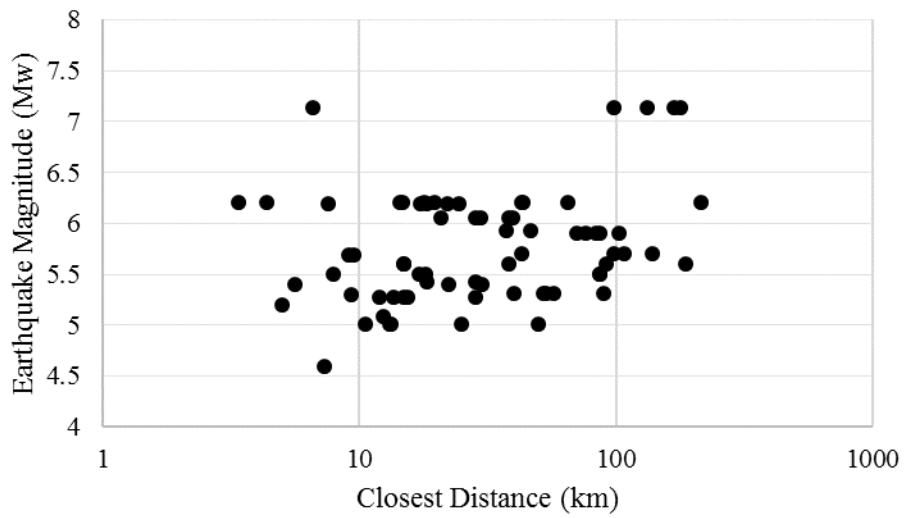
($M_w = 6.19$) at ZBR station following the Chalfant valley in 1986 was around 50% greater than those of the mainshock ($M_w = 5.8$).

The effects of aftershock selection were further explored through a numerical example and summarized in Chapter 4.2. Based on the conclusions drawn from this case study and given the increased number of aftershock records in the public domain, the use of as-recorded mainshock – aftershock sequences are considered more appropriate in this study.

In this research, a dataset was developed for as-recorded mainshock – aftershock sequences using the Next Generation Attenuation (NGA) strong motion database of the Pacific Earthquake Engineering Research Center (2014). In order to exclude structural dynamics, the ground motion records only from instruments located in ground level, basement, or free field were considered. This study requires as-recorded strong motion pairs of mainshock and aftershock; therefore, strong motions only from the same stations were used. The initial dataset included 144 strong motion pairs of mainshock-aftershock sequence with two orthogonal components from different parts of the world. As shown in Figure 8, the strong motion data include mainshocks ranging from $M_w = 5.6$ to 7.6 and aftershocks ranging from $M_w = 4.2$ to 7.1. The shear wave velocities were between 179 m/s to 1222 m/s, which corresponds to site classes B to E according to the preferred NEHRP site classification (Chiou, Darragh and Power 2005). Most of the mainshocks with $M_w > 7.5$ did not have aftershock records in the PEER database. Although very rare, it makes the database incomplete for strong aftershocks. The distribution of earthquake magnitude with respect to the distance is shown in Figure 8 for both mainshocks and aftershocks, respectively.



(a)



(b)

Figure 8: Earthquake magnitude distribution with respect to closest distance for selected (a) mainshocks and (b) aftershocks

Different earthquakes can also occur within a short time span. The short time frame between the events may cause them to be considered as a mainshock-aftershock

sequence. For example, Landers and Big bear earthquakes both occurred on June 28, 1992 with $M_w = 7.28$ and $M_w = 6.5$ respectively. In fact, these earthquakes were regional earthquakes and they were not considered as a mainshock – aftershock sequence by the seismologists (Wikipedia 2019).

Ground motions during an earthquake are characterized by ground motion parameters. Ground motion parameters represent characteristics of seismic loading including intensity, frequency content, and duration of the shock. The ground motion parameters considered in this study are peak ground acceleration (PGA), peak ground velocity (PGV), mean period (T_m), Arias intensity (I_a), and significant durations (D_{5-75} , D_{5-95}). Peak ground acceleration (PGA) represents the intensity of the earthquake. This represents the maximum value of ground acceleration recorded during an earthquake (Figure 9). The shortcoming of PGA is that it does not provide information on the frequency content or the duration of the motion. However, PGA as an intensity measure predicts the onset of sliding, and thus initially is more important than either frequency content or duration in sliding displacement prediction. A velocity-time history can be obtained by integrating the acceleration-time history over time. PGV is the peak of acceleration-time history. It includes some measure of the frequency content of the strong motion due to the numerical integration over time (Figure 9)

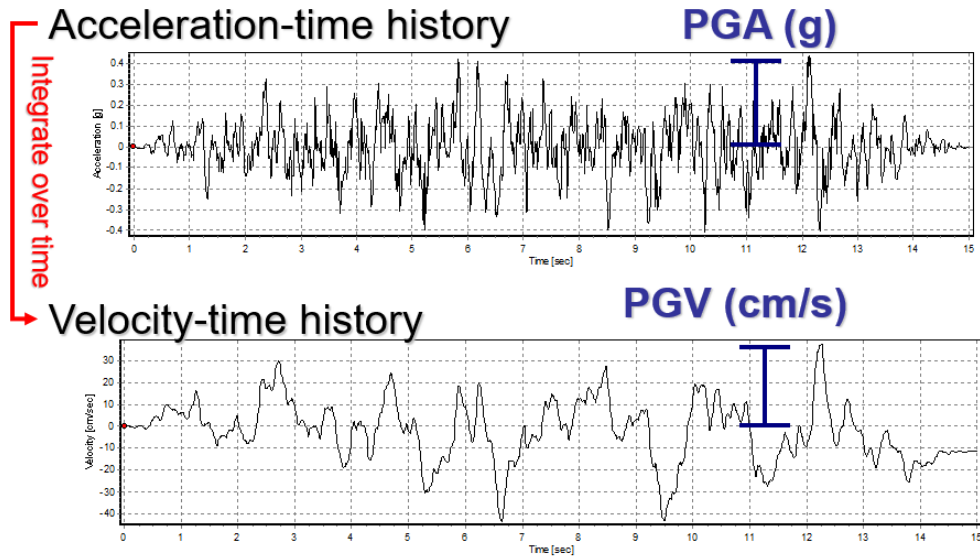


Figure 9: Acceleration and velocity time histories for an artificial strong motion record

The Arias Intensity (I_a) is obtained from the integration of squared accelerations from acceleration-time record (Arias 1970). The normalized I_a over time can be used to compute the significant duration parameters (i.e. D_{5-95} and D_{5-75}). Here, D_{5-75} means the time between 5% and the 75% of the total Arias Intensity. Figure 10 illustrates how I_a build up is used to compute duration parameters. Significant durations for the given hypothetical acceleration time history are $D_{5-95} = 10.32$ s and $D_{5-75} = 8.46$ s.

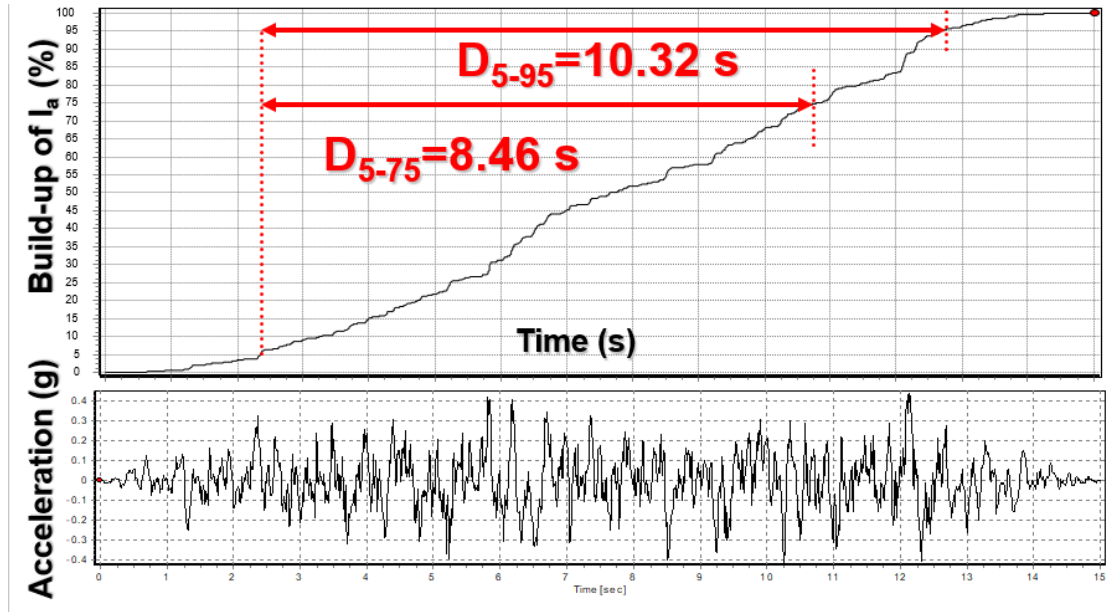


Figure 10: (a) Development of Arias Intensity over time (b) evaluation of significant durations (D_{5-95} and D_{5-75}) from the normalized Arias Intensity.

The dynamic response is significantly affected by the frequency content of the input ground motion such that if the frequency content of ground motion matches the natural period of the system, a resonance condition can develop, and significant damage can take place. The Mean Period (T_m) can be used to measure the frequency content of a ground motion [Rathje et al. (2014); Rathje et al. (2004)]. The distribution of these ground motion parameters among the selected mainshock and aftershock sequences is shown in Figure 11 and Figure 12.

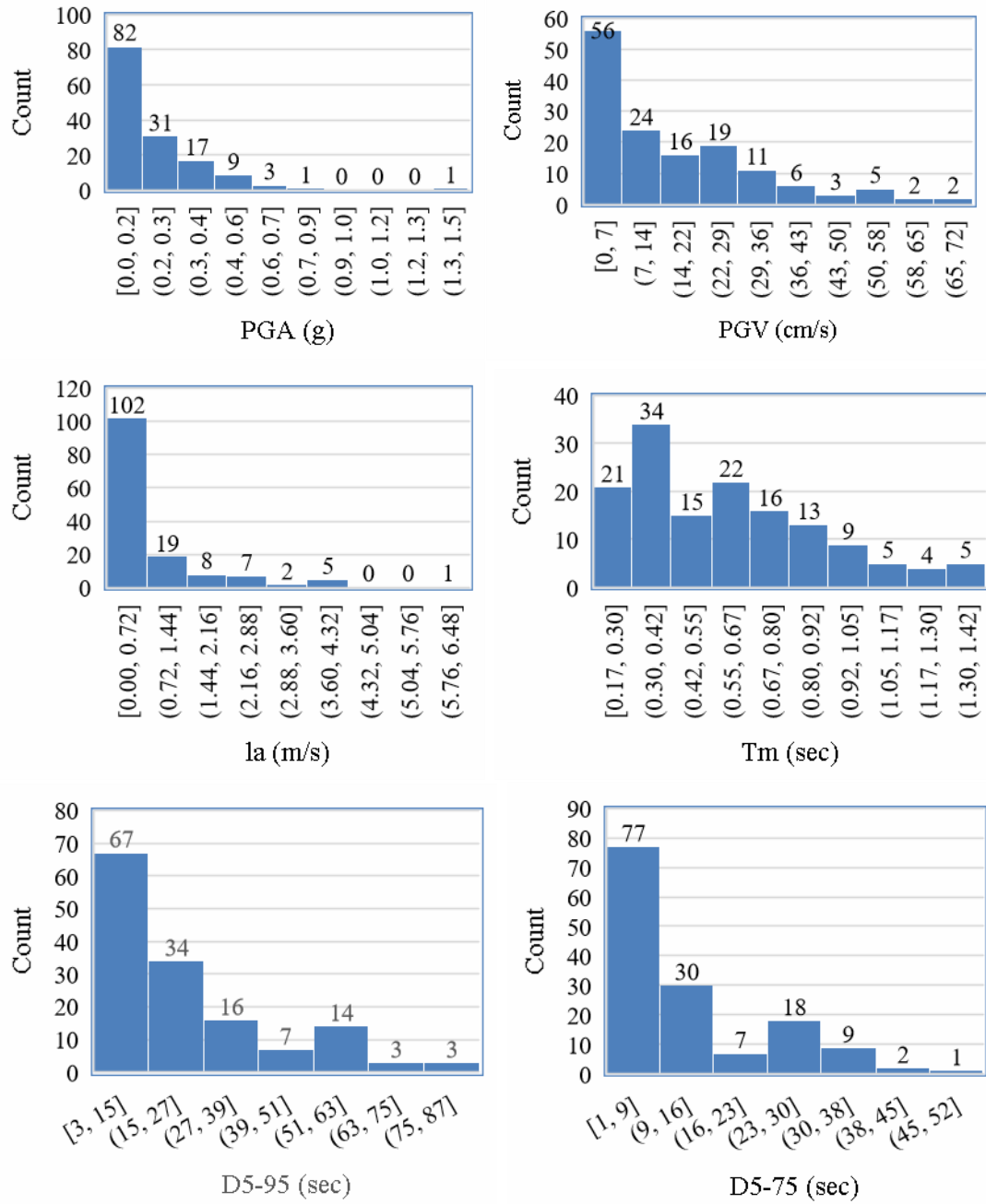


Figure 11: Distribution of Ground Motion Parameters PGA, PGV, Arias Intensity, Tm, D5-95, D5-75 for selected mainshocks.

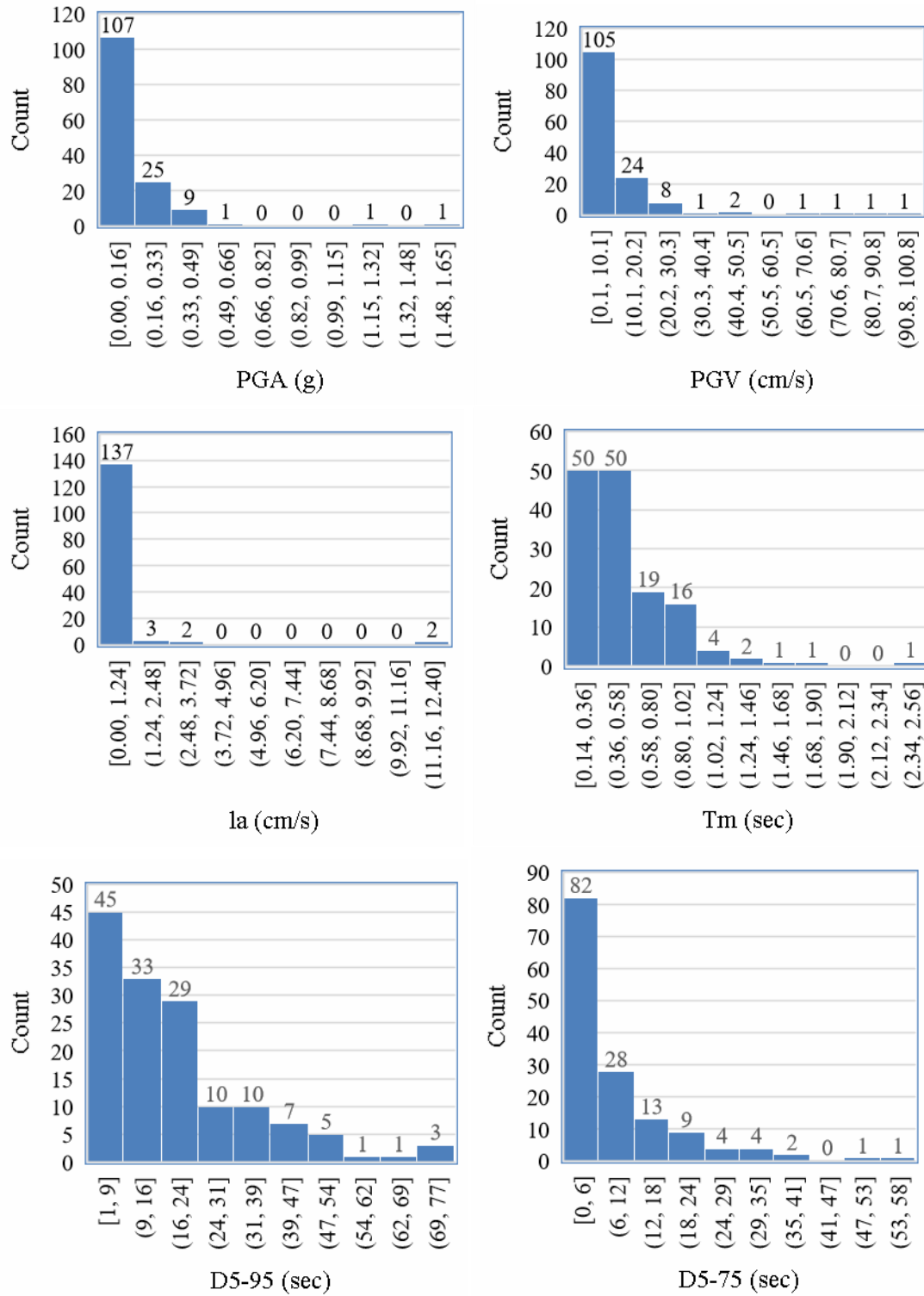


Figure 12: Distribution of Ground Motion Parameters PGA, PGV, Arias Intensity, Tm, D5-95, D5-75 for selected aftershocks.

Research Workflow

The main goal of this study is to improve the existing empirical models to predict the sliding displacements of flexible slopes subjected to mainshock – aftershock sequences. As the first step, site response analyses were performed on five hypothetical sites with site periods of 0.15 s, 0.3 s, 0.48 s, 1 sec, and 1.51 s using the dataset of 144 strong motion pairs of mainshock-aftershock sequences. A total of 720 1D linear equivalent linear site response analyses were performed. The details about the configuration of the hypothetical sites are presented by Antonakos (2009). Strata is a finite element software that utilizes equivalent-linear analysis method to obtain the response of a site for vertically propagating, horizontally polarized shear waves propagated through horizontal soil layers [Kottke and Rathje (2009)]. Strata is used to evaluate the dynamic response of flexible sliding masses and specifically to obtain the seismic loading parameters (k_{\max} , $k\text{-vel}_{\max}$) and k -time history at the base of sliding mass.

Secondly, decoupled sliding displacements were calculated using the k -time histories of the aforementioned 720 cases. Here, decoupled sliding displacements were calculated for three yield accelerations including 0.04 g, 0.08 g and 0.16 g. Sliding displacements were computed using the SLAMMER program (2013). The resulting dataset consisted of 968 non-zero sliding displacement values for mainshocks and 394 non-zero displacements for recorded aftershocks.

Summary

In this chapter, a comprehensive dataset including strong ground motion records from a total of 144 mainshocks and their corresponding aftershocks was generated. The strong motion data is collected from the PEER database. This chapter also describes the

research workflow to perform dynamic response and sliding displacement analyses at various site and slope conditions.

Chapter Four

Dynamic response and sliding displacement analyses

Introduction

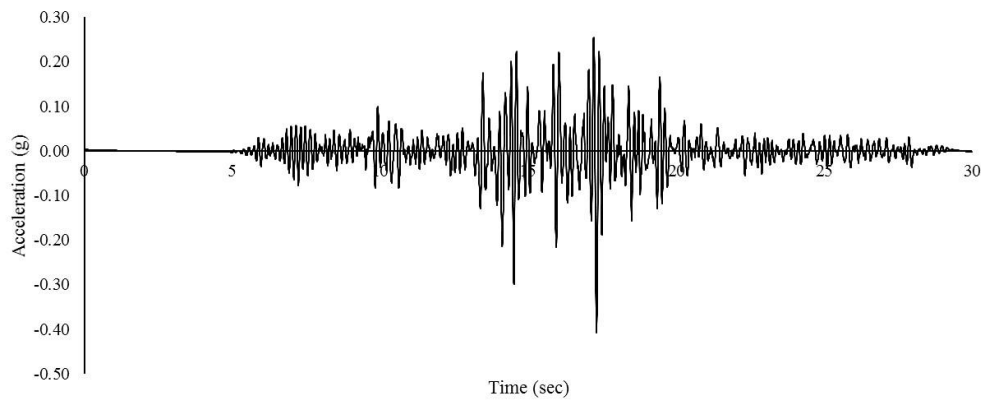
The main objective of this chapter is to verify the accuracy of the existing empirical models for the seismic loading parameters and sliding displacements for flexible slopes. The organization of this chapter is such that first the calculation procedure for the seismic loading parameters are presented. Next, the results of dynamic response and decoupled sliding displacement analyses are presented. Finally, the effects for aftershock record selection is discussed.

There are readily available empirical models assisting engineers to predict the dynamic response of soils without performing site response analyses. As compared to the datasets of previous studies, the dataset developed in this research includes a new subset of earthquake strong motion records from the PEER database. This dataset provides a unique opportunity to (i) verify the validity of existing predictive models and (ii) assess if there is any dataset bias in the predictions of previous studies. Following the framework proposed by Rathje and Antonakos (2011), new empirical relationships are developed for the seismic loading parameters (k_{\max} and $k\text{-vel}_{\max}$) for verification purposes only to compare the results with the available empirical models. Rathje and Antonakos (2011) developed empirical models for k_{\max} and $k\text{-vel}_{\max}$ using the results of 400 1-D site response analyses. These models predict k_{\max} and $k\text{-vel}_{\max}$ as functions of the PGA, PGV and T_m of the input motion and the natural period of the sliding mass (T_s). They extended the (PGA, PGV) rigid sliding displacement model of Saygili and Rathje (2008) to make it applicable to flexible sliding masses. The extension involves using k_{\max} and $k\text{-vel}_{\max}$ in place of PGA and PGV in the original

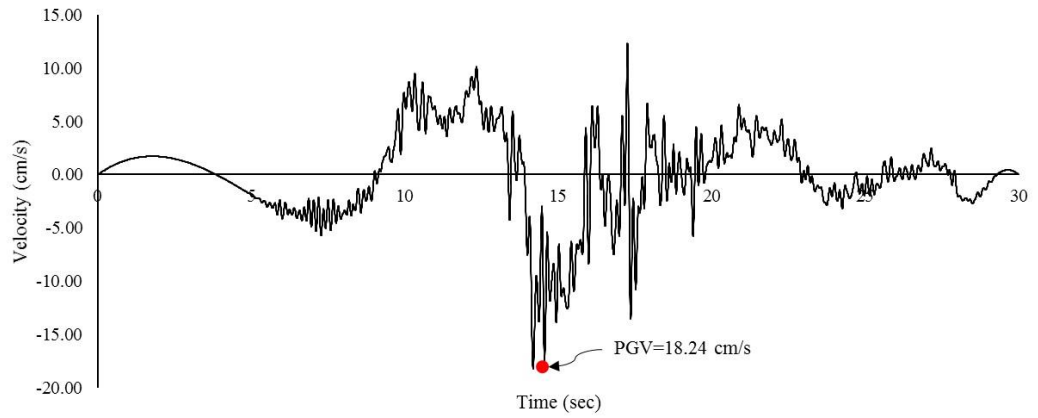
(PGA, PGV) vector model, and the addition of the natural period of the sliding mass T_s . In this study, a total of 720 1D linear equivalent linear site response analyses were performed on 5 hypothetical sites using 144 earthquake strong motion records. The procedures proposed by Saygili and Rathje (2008) and Rathje and Antonakos (2011) are followed for the development of the predictive models for the seismic loading parameters.

Calculation of the seismic loading parameters

The fundamental change on the Rathje and Antonakaos (2011) is the development of the seismic loading parameters (k_{max} , $k\text{-vel}_{max}$). This section briefly demonstrates the procedure to compute these parameters. To demonstrate the calculation of k_{max} and $k\text{-vel}_{max}$ ARE000 motion of 1999 Koceali earthquake (M_w 7.51, $R_{closest} = 13.49$ km, and $V_{s,30} = 523$ m/sec) was considered. As displayed in Figure 13, the velocity – time history was obtained by numerically integrating the acceleration-time history over time. The PGA is equal to 0.41g and PGV is equal to 18.24 cm/sec.



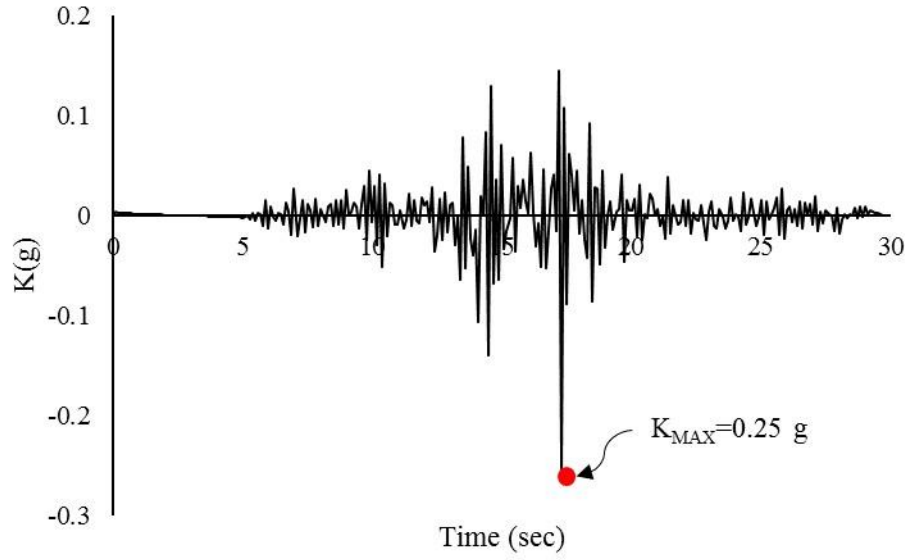
(a)



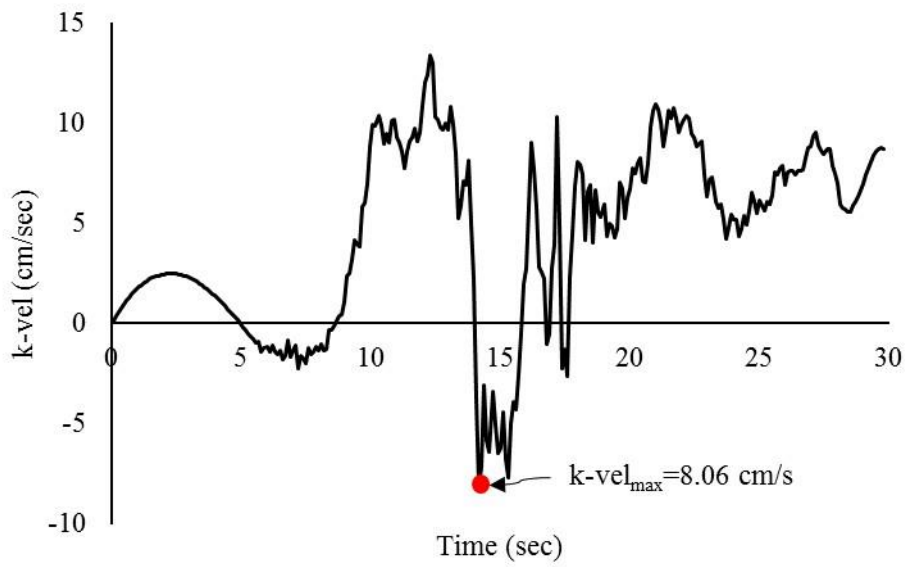
(b)

Figure 13: (a) Acceleration-time history and (b) Velocity-time history for ARE000.

A dynamic response analyses was performed to obtain the k-time history for Site A ($V_s = 400$ m/sec, $T_s=0.15$ sec) for the ARE000 motion. As displayed in Figure 14, the k-vel time history was calculated by integrating the k-time history over time. The $k_{\max} = 1.25$ g represents the seismic demand on the deformable sliding mass and it is less than the $PGA = 0.41$ g due to averaging of accelerations. Similarly, for $k\text{-vel}_{\max} = 8.06$ cm/s is smaller than PGV value of 18.24 cm/s original motion.



(a)



(b)

Figure 14: The k-time history and k-vel – time history of site A for ARE000 motion

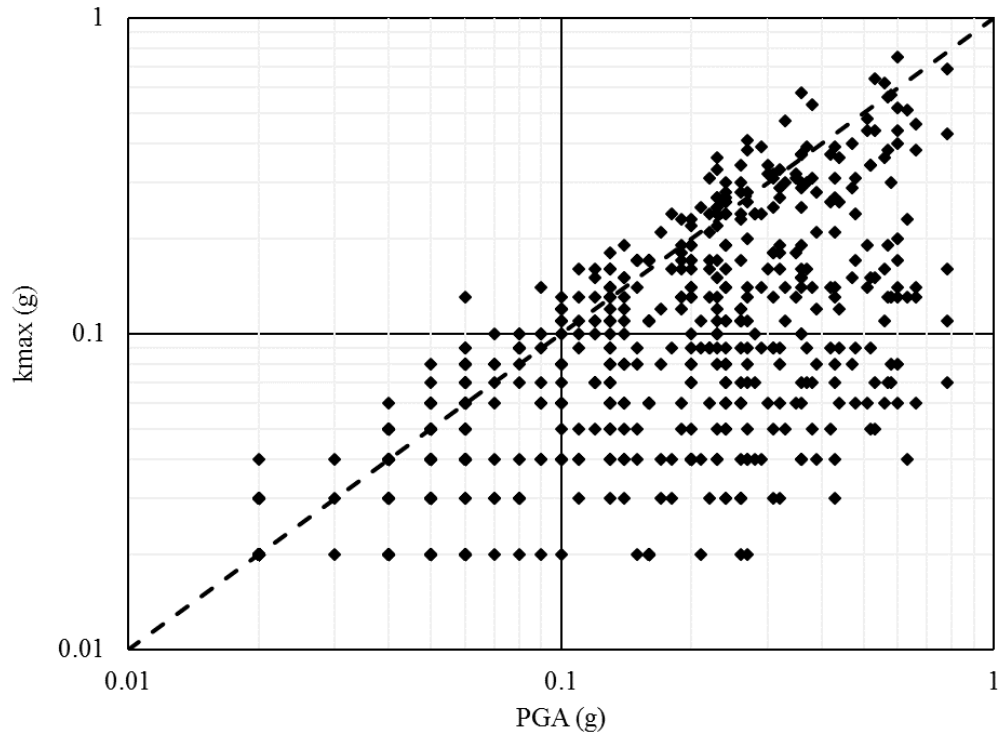
A parametric sensitivity was performed to investigate the impact of ground motion parameters (PGA, PGV, and T_m) and site parameter (T_s) on the seismic loading

parameters k_{\max} and $k\text{-vel}_{\max}$ by changing the value of one parameter at a time. The following observations were made from this sensitivity study:

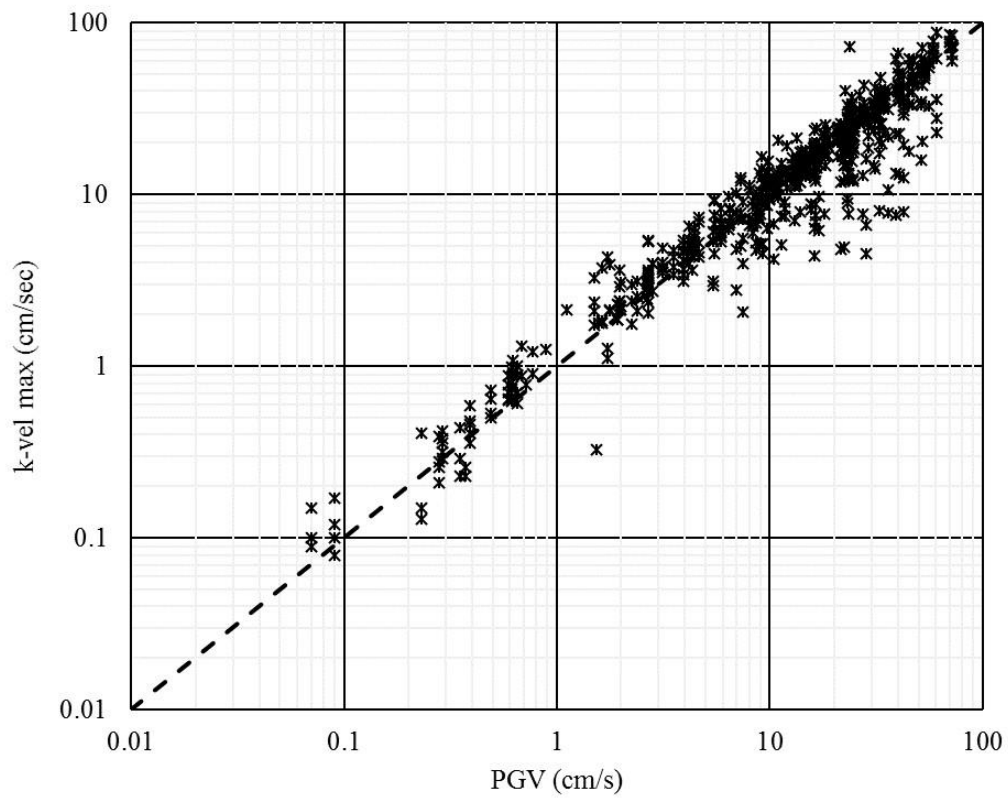
- Given the same T_m and T_s values, k_{\max} increased with an increase in PGA; however, the ratio of k_{\max}/PGA decreased with increased intensity.
- When the ground motion parameters (PGA, PGV and T_m) were kept constant and only T_s was changed, the site with lower site period showed relatively higher k_{\max} and $k\text{-vel}_{\max}$ values.
- Both k_{\max}/PGA and $k\text{-vel}_{\max}/\text{PGV}$ increased with an increase in T_m

Verification of existing predictive models for dynamic response

The previous section presented the procedure to obtain the seismic loading parameters. The seismic loading parameters (k_{\max} and $k\text{-vel}_{\max}$) are significantly correlated with the intensity of the input strong motion. Figure 15 displays k_{\max} and $k\text{-vel}_{\max}$ as functions of PGA and PGV of the original ground motion, respectively. As expected, the trends of the data suggest that k_{\max} increases with PGA with a diminishing trend whereas $k\text{-vel}_{\max}$ is very similar to PGV at all PGV levels.



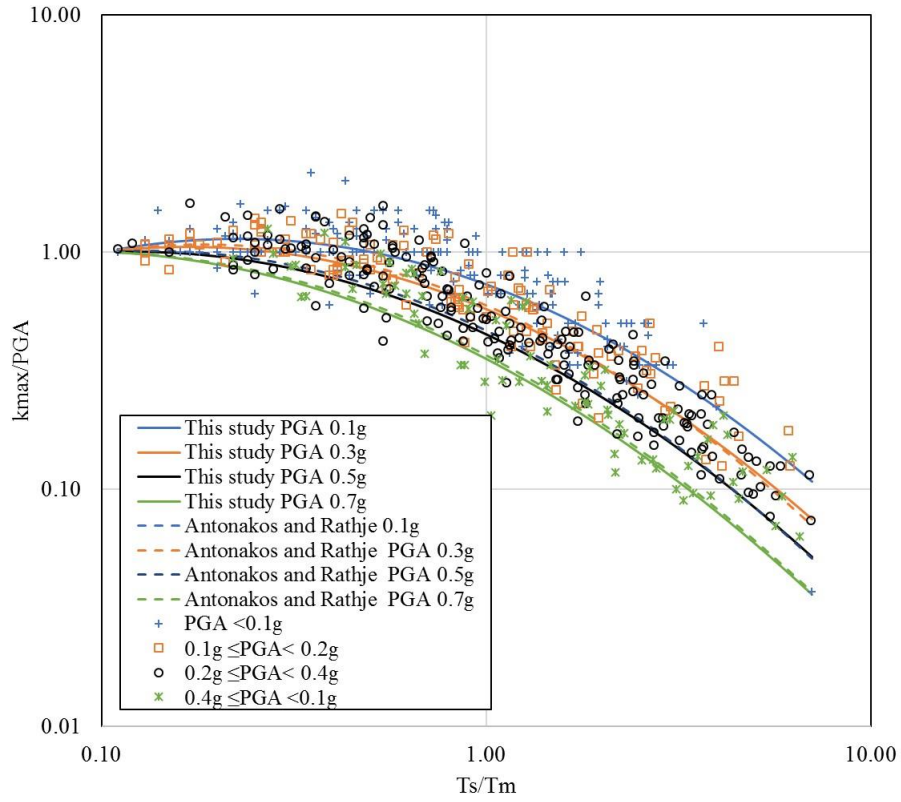
(a)



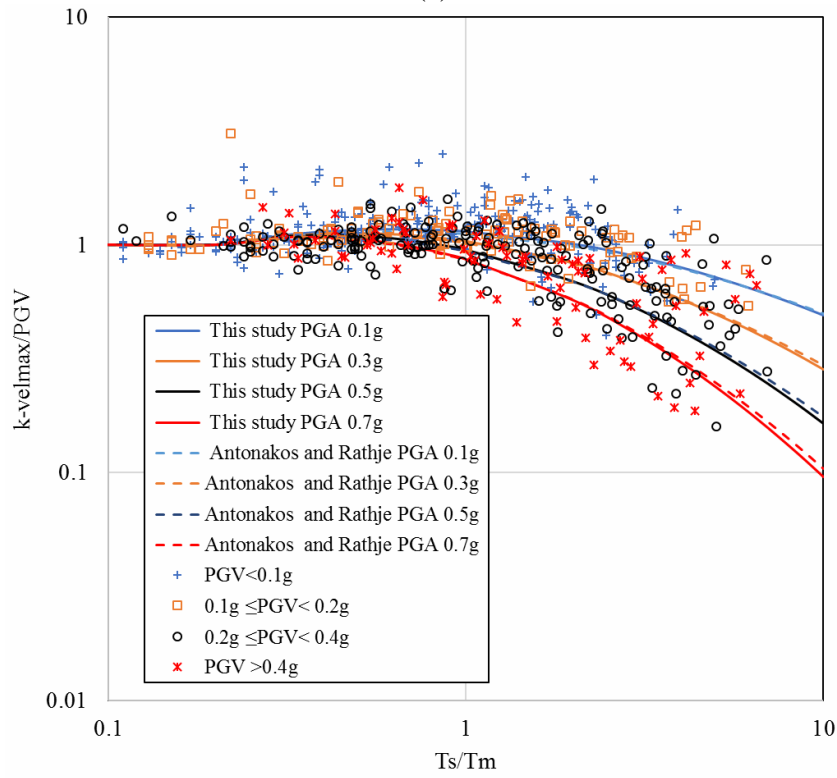
(b)

Figure 15: Distribution of (a) k_{\max} versus corresponding PGA and (b) $k\text{-vel}_{\max}$ versus corresponding to PGV

In accordance with the observations by Rathje and Antonakos (2011), k_{\max} and $k\text{-vel}_{\max}$ increase with the frequency content of the input earthquake ground motion but decrease with the fundamental site period. To account for this opposite trend, Rathje and Antonakos (2011) introduced a period ratio term (i.e. T_s/T_m) in the functional form of their predicted models to further reduce the variability. Figure 16 shows k_{\max}/PGA and $k\text{-vel}_{\max}/\text{PGV}$ as functions of the period ratio for different PGA bins. On average both k_{\max}/PGA and $k\text{-vel}_{\max}/\text{PGV}$ ratios are close to unity at small period ratios. This common trend suggests that sliding masses are acting as rigid bodies at small period ratios. Following a 2nd degree polynomial functional form in log-log space as suggested by Rathje and Antonakos (2011), statistical analyses are performed to compute the regression coefficients for k_{\max} and $k\text{-vel}_{\max}$ models. JMP (2018) statistical package is utilized for this task. In Figure 16, the predictions of the resulting k_{\max} and $k\text{-vel}_{\max}$ models are compared to those of the Antonakos and Rathje (2011) models. As shown by continuous and dashed lines, the predictions of the models developed in this study are almost coincident with the Rathje and Antonakos (2011) models at all PGA levels and period ratios. The comparison of the predictions of two models with different datasets clearly indicates that there is no dataset bias in these models.



(a)



(b)

Figure 16: Variation of (a) k_{\max}/PGA and (b) $k\text{-vel}_{\max}/PGV$ versus T_s/T_m .

As the next step, an attempt has been made to improve the accuracy of the models and reduce the uncertainty parameters (i.e. standard deviation) by changing the functional forms of the predictive equations. However, the inclusion of higher-order terms did not significantly change the goodness of the fits as well as the standard deviation of the predictions. The final forms of the predictive models are summarized in Equations 1 and 2.

$$\ln\left(\frac{k_{\max}}{PGA}\right) = (0.406 - 0.718 \cdot PGA) \cdot \ln\left(\frac{k_{\max}}{PGA}\right) + (-0.212 + 0.080 \cdot PGA) \cdot \left(\ln\left(\frac{T_s}{T_m}\right)\right)^2 \quad (1)$$

$$\ln\left(\frac{k\text{-vel}_{\max}}{PGV}\right) = 0.27 \cdot \ln\left(\frac{k\text{-vel}_{\max}}{PGV}\right) + (-0.10 - 0.18 \cdot PGA) \cdot \left(\ln\left(\frac{T_s}{T_m}\right)\right)^2 \quad (2)$$

Where k_{\max} and $k\text{-vel}_{\max}$ are seismic shaking parameters in units g and cm/sec respectively, PGA is the peak ground acceleration in units of g, PGV is the peak ground velocity in units of cm/s, T_s is the site period in seconds, and T_m is mean period of the ground motion. The resulting standard deviation of the k_{\max}/PGA model was 0.260 (in natural log units) for this study and 0.245 (in natural log units) for Rathje and Antonakos (2011) model. The resulting standard deviation of the $k\text{-vel}_{\max}/PGV$ model was 0.27 (in natural log units) for this study and 0.25 (in natural log units) for Rathje and Antonakos (2011) model.

Sliding Displacement Analyses

The k-time histories of 720 aforementioned cases for 5 different site conditions were used to compute decoupled sliding displacements for three yield accelerations (0.04 g, 0.08 g, and 0.16 g). Following the sliding block methodology, decoupled sliding displacements were computed using the SLAMMER program (2013). The resulting

dataset consisted of 968 non-zero sliding displacement values for mainshocks and 394 non-zero displacements for recorded aftershocks. The reason for a larger non-zero sliding displacement dataset for mainshocks than aftershocks is that on average mainshocks are stronger than aftershocks as shown in Figure 8. Hence, mainshocks induce greater sliding displacements than aftershock.

Decoupled sliding displacements were calculated for mainshocks using scalar model (k_{\max} , M) and the vector model (i.e. k_{\max} , $k\text{-vel}_{\max}$) for flexible slopes (Rathje, et al. 2014). The k_{\max} , M model for flexible sliding displacement and its standard deviation is given in Equation 3 and the k_{\max} , $k\text{-vel}_{\max}$ model for flexible sliding displacement and its standard deviation is given in Equation 4.

$$D = 4.89 - 4.85 \left(\frac{a_{\max}}{g} \right) - 19.64 \left(\frac{a_{\max}}{g} \right)^2 + 42.49 \left(\frac{a_{\max}}{g} \right)^3 - 29.06 \left(\frac{a_{\max}}{g} \right)^4 \quad (3a)$$

$$+ 0.72 \ln(a_{\max}) + 0.89(M - 6) + \begin{cases} 3.69 \cdot T_s - 1.22 \cdot T_s^2 & T_s \leq 1.5 \text{ s} \\ 2.78 & T_s > 1.5 \text{ s} \end{cases}$$

$$\sigma_{D,D}(a_{\max}, M) = 0.694 + 0.32 \left(\frac{a_{\max}}{g} \right) \quad (3b)$$

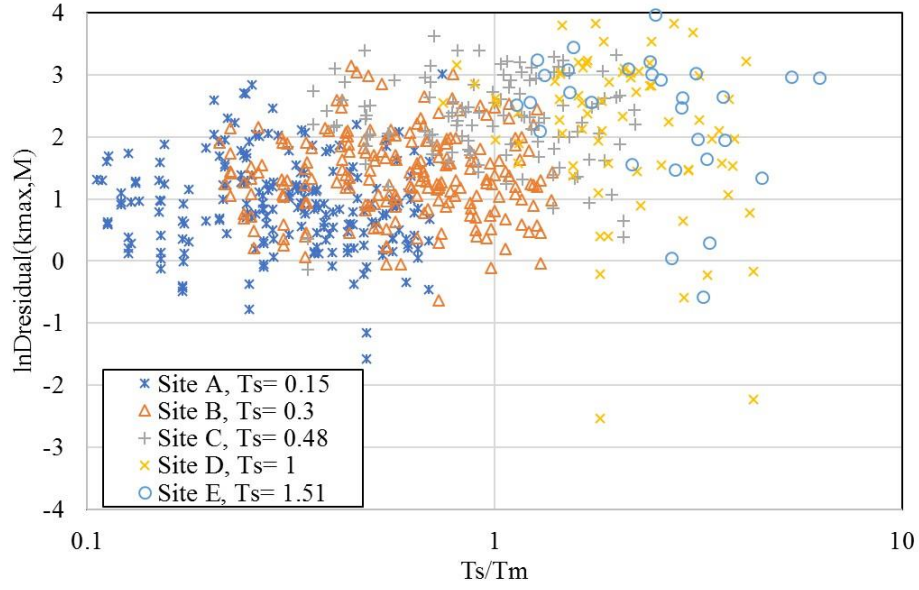
$$D = -1.56 - 4.58 \left(\frac{a_{\max}}{g} \right) - 20.84 \left(\frac{a_{\max}}{g} \right)^2 + 44.75 \left(\frac{a_{\max}}{g} \right)^3 - 30.50 \left(\frac{a_{\max}}{g} \right)^4 \quad (4a)$$

$$D = -1.56 - 4.58 \left(\frac{a_{\max}}{g} \right) - 20.84 \left(\frac{a_{\max}}{g} \right)^2 + 44.75 \left(\frac{a_{\max}}{g} \right)^3 - 30.50 \left(\frac{a_{\max}}{g} \right)^4 \quad (4b)$$

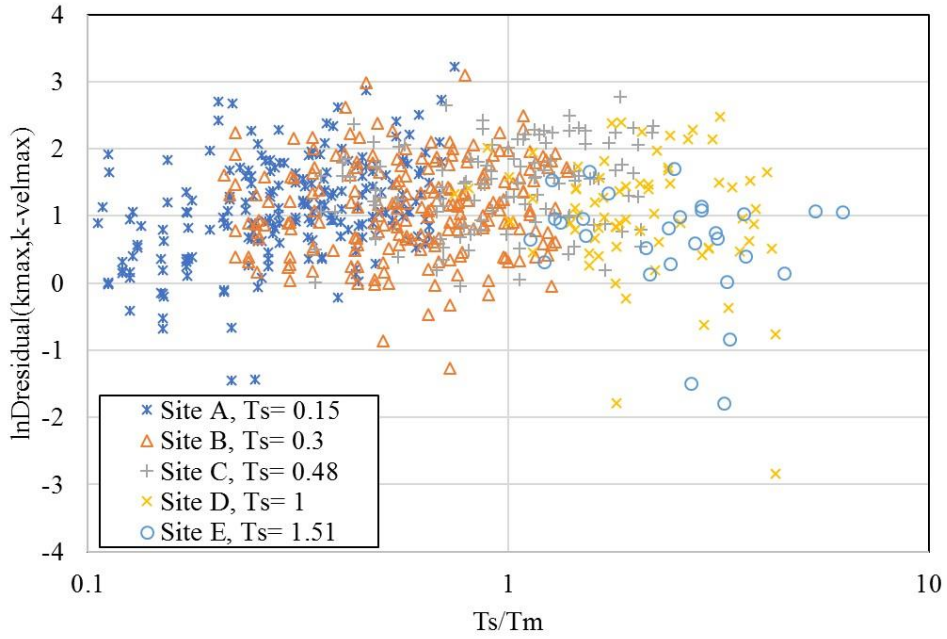
$$- 0.64 \ln(a_{\max}) + 1.55 \ln(-ve a_{\max}) + \begin{cases} 1.42 \cdot T_s & T_s \leq 0.5 \text{ s} \\ 0.71 & T_s > 0.5 \text{ s} \end{cases}$$

$$\sigma_{D,D}(a_{\max}, -ve a_{\max}) = 0.40 + 0.22 \left(\frac{a_{\max}}{g} \right)$$

Where D is displacement in cm, M is the magnitude, k_y is the yield acceleration in g, k_{\max} and $k\text{-vel}_{\max}$ are seismic shaking parameters in units g and cm/sec, respectively. These empirical models were developed using recorded motions from active tectonic regions and do not accompany aftershock records. Residuals ($\ln D_{\text{computed}} - \ln D_{\text{predicted}}$) stand for the difference between the computed and predicted displacements in natural logarithm units. Residuals of the (k_{\max}, M) model and the $(k_{\max}, k\text{-vel}_{\max})$ model are shown as functions of the period ratio in Figure 17. The trend of the data suggests that period ratio is not an omitted parameter as residuals do not vary with period ratio.



(a)

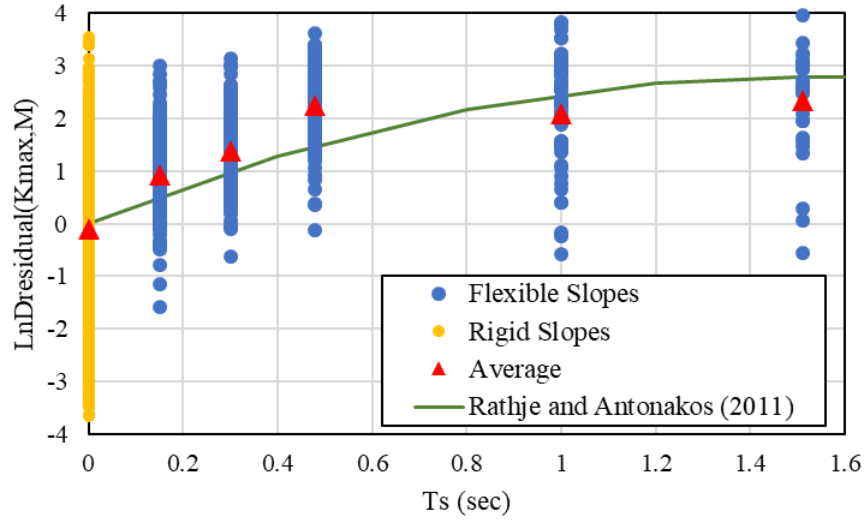


(b)

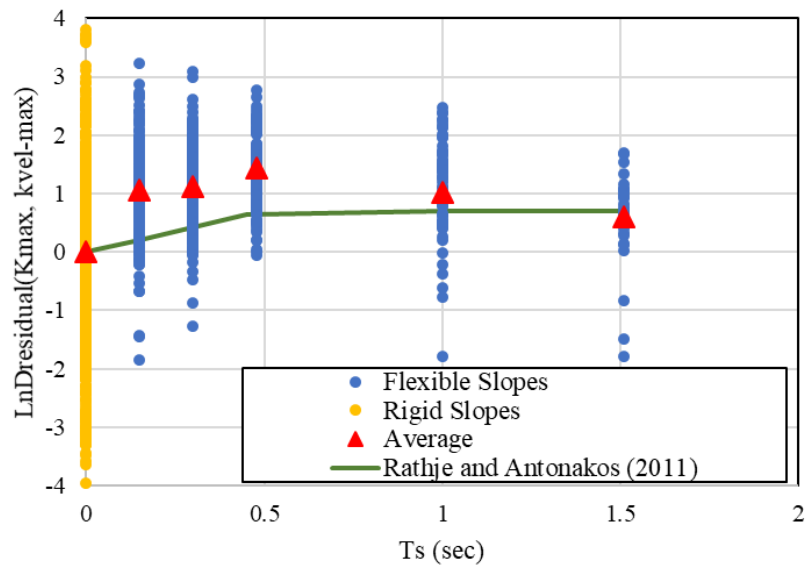
Figure 17: Displacement residuals (a) scalar model and (b) vector model versus T_s/T_m

Figure 18 shows the residuals of the (k_{\max}, M) model and the $(k_{\max}, k\text{-vel}_{\max})$ model as functions of the site period in Figure 18. It also shows the sliding displacement predictions for rigid slopes ($T_s = 0$). Rathje and Antonakos (2011) documented that

residuals slightly increase with increasing site period. The average of the residuals from this study compares well with the trend observed by Rathje and Antonakos (2011).



(a)



(b)

Figure 18: Displacement residuals versus the site period for (a) k_{max} , M model and (b) k_{max} , $k\text{-vel}_{max}$ model

Aftershock record selection

There are two common practices to represent the strong motion data for mainshock – aftershock sequences. These are the use of artificial time histories and as-recorded time histories. Artificial time histories are generated by scaling mainshock records as aftershocks. Here, the frequency content and duration characteristics are assumed to be the same. In essence, the ground motion characteristics of the mainshock and aftershocks can be remarkably different than each other. In this section, a case study is presented to illustrate the effects of aftershocks on earth slopes. A dataset was developed using 144 pairs of artificial and as-recorded mainshock – aftershock sequences using PEER database.

As the first step, decoupled sliding displacements were computed using as-recorded mainshock – aftershock sequences. The mainshocks were then scaled to match aftershocks by the PGV ratio (defined as $PGV_{\text{aftershock}}/PGV_{\text{mainshock}}$). The scaled mainshocks are labelled as “artificial aftershocks”. A comparison of the sliding displacements from artificial aftershocks and as-measured aftershocks in Figure 19 reveals that the overall trend of the data (represented by red dashed line) is above the 45-degree line for sliding displacements smaller than 7.5 cm (i.e., $\ln D = 2$) and it is below the 45-degree line for sliding displacements greater than 7.5 cm (i.e., $\ln D = 2$). The interpretation of this inconsistent trend is that sliding displacements from artificial aftershocks can lead to significant overestimation of the seismic demand parameters for earth slopes at relatively small displacement levels and can lead to un-conservative estimation of the seismic demand parameters for earth slopes at relatively large displacement levels. Therefore, as-recorded master mainshock – aftershock sequences were used in this research.

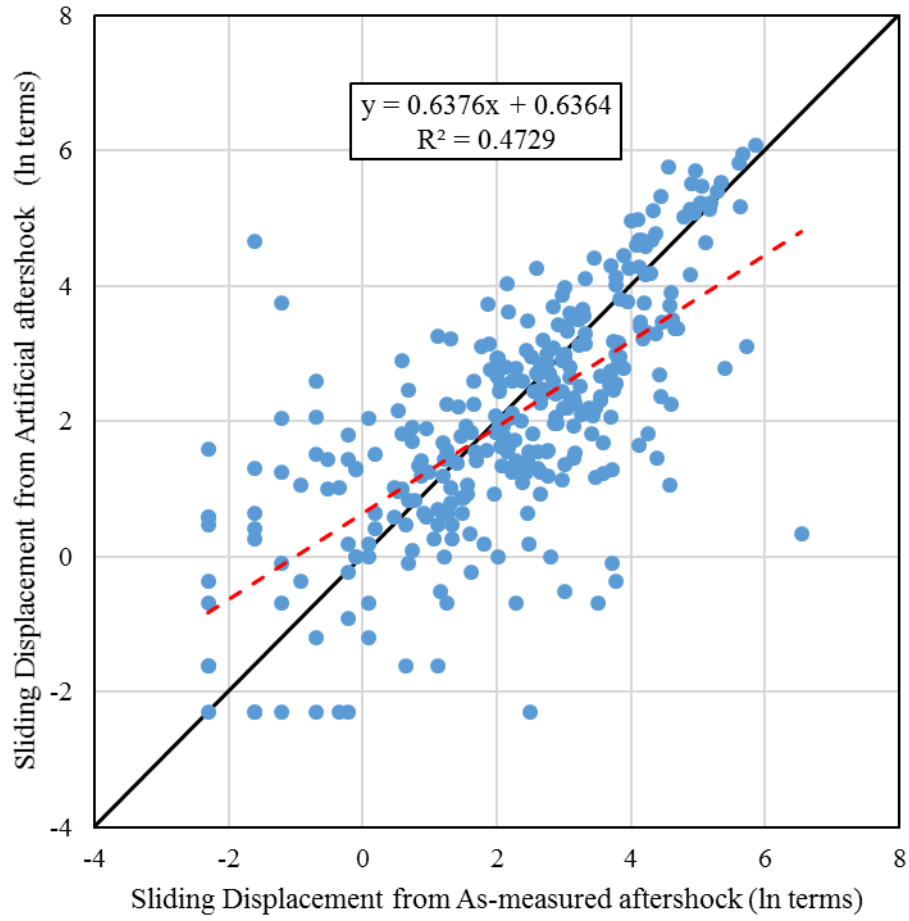


Figure 19 : Artificial aftershock displacement versus Recorded aftershock displacement

Summary

This chapter presents the results of the dynamic response and sliding displacement analyses performed throughout this research. The database is utilized to verify the accuracy of the existing predictive models for the dynamic response of flexible soils. Decouple sliding displacements were calculated for mainshocks using scalar model (k_{\max} , M) and the vector model (i.e. k_{\max} , $k\text{-vel}_{\max}$) for flexible slopes. Sliding displacements obtained from artificial aftershocks were found to be less conservative

as compared to the sliding displacements obtained from as-recorded aftershocks for higher displacement levels. A better correlation was observed between the artificial aftershocks and PGV factor as compared to as-recorded aftershocks and PGV factor.

Chapter Five

Effects of Aftershocks

Introduction

The results presented in the previous chapter focused on the results of the dynamic response and decoupled sliding displacement analyses for sliding masses subjected to mainshocks only. In essence, recent research reveals that mainshocks may cause elongation of the site period of flexible sliding masses and the frequency contents of aftershocks can be significantly different than the mainshock [Wang (2014) ; Rathje et al. (2014)]. The seismic risks associated with the aftershocks is also significant as aftershocks are subjected to post-mainshock (“damaged”) slopes.

Various empirical models are available that predict sliding displacement as a function of ground motion parameters and site parameters but the data sets for these empirical models do not accompany aftershock records. The objective of this chapter is to incorporate the aftershock effects on the recently developed predictive models for flexible sliding masses. Decoupled sliding displacements that considers mainshocks exclusively are used for the investigation of the effects of aftershocks.

Development of sliding displacement predictive models that incorporate aftershocks

Decoupled sliding displacements were calculated using the 720 k-time histories for 5 site conditions with 3 yield accelerations (0.04 g, 0.08 g, and 0.16 g). The resulting dataset consisted of 968 non-zero sliding displacement values for mainshocks. To incorporate the effects of mainshock – aftershock sequences, aftershocks are applied on post-mainshock “damaged” slopes and decoupled sliding displacements were

calculated. The resulting dataset consisted of 394 non-zero displacements for recorded aftershocks.

Rathje et al. (2014) presented the sensitivity of predicted k_{\max} , $k\text{-vel}_{\max}$, and sliding displacement to the site period through a hypothetical case study where the ground shaking is characterized by a $M_w = 7$, $R = 5$ km event with $\text{PGA} = 0.35$ g, $\text{PGV} = 30$ cm/s, and $T_m = 0.45$ s (Figure 20). Here, sliding displacements generally decrease at larger values of site periods as k_{\max} decreases and the displacements approach zero as k_{\max} approaches the yield acceleration (k_y). Mainshocks typically cause elongation of site period of flexible slopes; therefore, it may be assumed that post-mainshock slopes can stay stable following aftershocks as they exert a relatively low seismic demand on the slope compared to the mainshock. In essence, this assumption is not necessarily correct because post-mainshock slopes can be more fragile when subjected to aftershocks due to the “damage” from the mainshock.

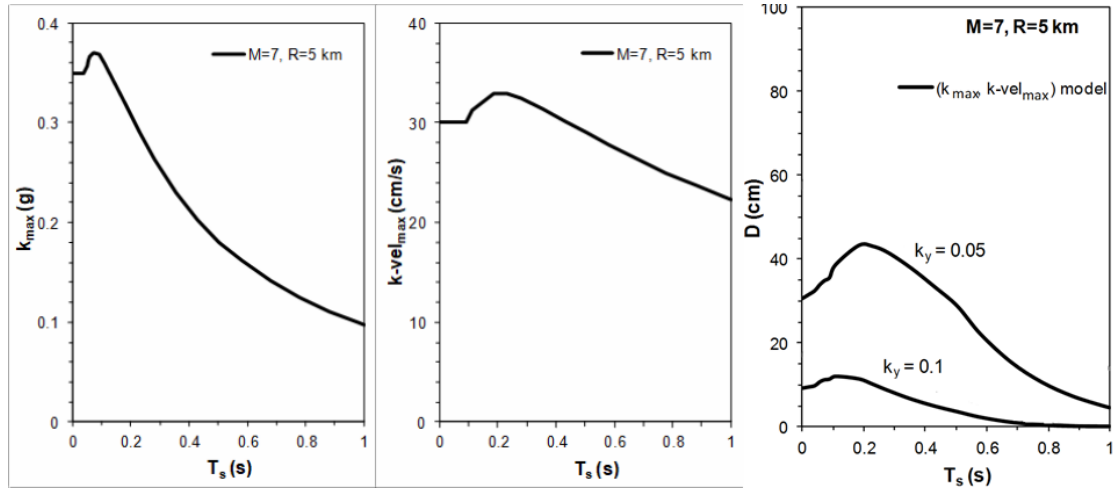


Figure 20: Predicted (a) k_{max} , (b) $k-vel_{max}$, and (c) sliding displacements as a function of the natural period of the sliding mass for a $M=7$, $R=5$ km event (Rathje, Wang, et al. 2014)

In his third McClelland Keynote Lecture, Andersen (2015) introduced a strain-based strength degradation procedure to predict post-mainshock yield accelerations of “damaged” slopes. An assessment of the yield accelerations of post-mainshock slopes is beyond the scope of this research; therefore, a parametric sensitivity is performed to evaluate yield strength degradation. The engineering properties of soils are strain-rate dependent. Skempton (1985) suggested a 5% variation when the loading condition changes from static to dynamic conditions. Recent research documented that the friction angle of the post-mainshock slopes are on average are 2% to 8% smaller than those of intact slopes[Wu and Tsai (2011); Tiwari et al. (2005); Kim et al. (2004)]. This observation corresponds to a decrease in the yield acceleration by 5% to 20% using an infinite slope approximation. Used as an index of the aftershock damage, sliding displacements on post-mainshock slopes were predicted using 4 levels of yield acceleration reduction factors (i.e. $\Delta k_y = 5\%$, 10% , 15% , and 20%).

The resulting dataset consisted of 394 non-zero displacements for recorded aftershocks at different site periods. As summarized in Table 1, expected sliding displacements on post-mainshock slopes subjected to aftershocks increased on average around 30% at all site periods. Figure 21 displays that decoupled sliding displacements in aftershock environment increase with an increase in site periods. The sliding displacement increase is due to the combined effects of strength degradation and the additional seismic demand by the aftershock. Overall, the results suggest that aftershocks may increase the seismic demand relative to the mainshock alone; thus, the seismic risk may be underestimated if aftershocks are neglected.

Table 1: Percent increase in decoupled sliding displacements in aftershock environment

Site Name	$\Delta k_y=5\%$	$\Delta k_y=10\%$	$\Delta k_y=15\%$	$\Delta k_y=20\%$
Site A	27%	27%	29%	31%
Site B	40%	34%	34%	26%
Site C	34%	36%	35%	36%
Site D	34%	25%	43%	43%
Site E	41%	30%	26%	58%
Overall	35%	30%	33%	39%

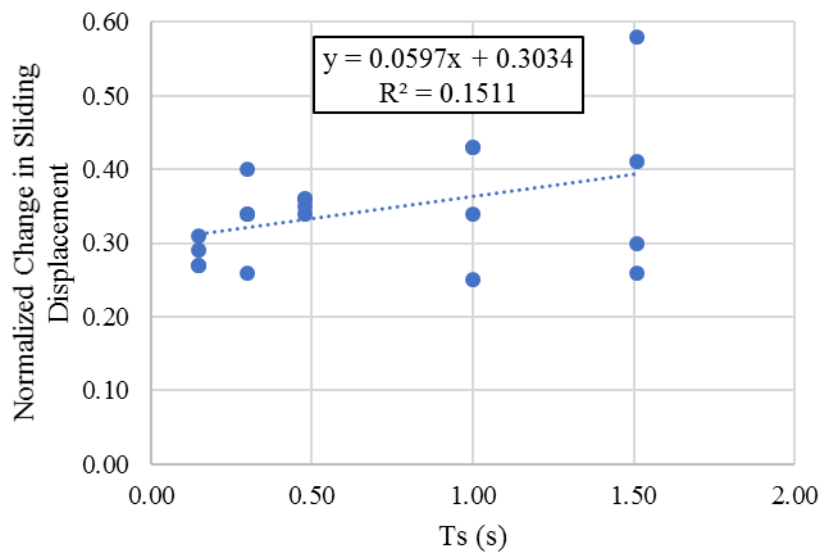


Figure 21: Decoupled sliding displacement increase due to aftershocks

In an attempt to properly address the aftershock damage, the original flexible sliding displacement models proposed by Rathje et al. (2014) are modified to include the strength degradation on the yield acceleration of post-mainshock slopes as follows:

$$\begin{aligned}
 D = & 0.597T_s + 0.3034 + 4.89 - 4.85 \left(\frac{k_{y,ma}}{k_{y,s}} \right) - 19.64 \left(\frac{k_{y,ma}^2}{k_{y,s}^2} \right) + \\
 & 42.49 \left(\frac{k_{y,ma}}{k_{y,s}} \right)^3 - 29.06 \left(\frac{k_{y,ma}}{k_{y,s}} \right)^4 \\
 & 3.69 \cdot \frac{k_{y,ma}}{k_{y,s}} - 1.22 \cdot T_s^2 \quad \text{for } T_s \leq 1.5 \text{ s} \\
 & + 0.72 \ln(k_{y,ma}) + 0.89(M - 6) + 2.78 \quad \text{for } T_s > 1.5 \text{ s} \\
 \{ &
 \end{aligned}
 \tag{4a}$$

$$\begin{aligned}
 D = & 0.597T_s + 0.3034 - 1.56 - 4.58 \left(\frac{k_{y,ma}}{k_{y,s}} \right) - 20.84 \left(\frac{k_{y,ma}^2}{k_{y,s}^2} \right) + \\
 & 44.75 \left(\frac{k_{y,ma}}{k_{y,s}} \right)^3 - 30.50 \left(\frac{k_{y,ma}}{k_{y,s}} \right)^4 \\
 & 1.42 \cdot \frac{k_{y,ma}}{k_{y,s}} \quad \text{for } T_s \leq 0.5 \text{ s} \\
 & -0.64 \ln(k_{y,ma}) + 1.55 \ln(k_{y,s} - v e^{-k_{y,ma}}) + \{ 0.71 T_s \quad \text{for } T_s > 0.5 \text{ s} \\
 \{ &
 \end{aligned}
 \tag{4b}$$

Where D is displacement in cm, M is the magnitude, k_y is the yield acceleration in g, and k_{\max} and $k\text{-vel}_{\max}$ are seismic shaking parameters in units g and cm/sec, respectively.

To present the impact of the mainshock – aftershock sequence, decoupled sliding displacements were predicted for a mainshock only case (Equation 3) and for mainshock – aftershock sequence (Equation 4) for a seismic event with a PGA=0.35 g, PGV = 30 cm/sec, and $T_m=0.45$ s. Here, the dynamic response of the sliding mass was predicted using Equation 1 and Equation 2. As summarized in Figure 22, decoupled sliding displacements were greater in the aftershock environment.

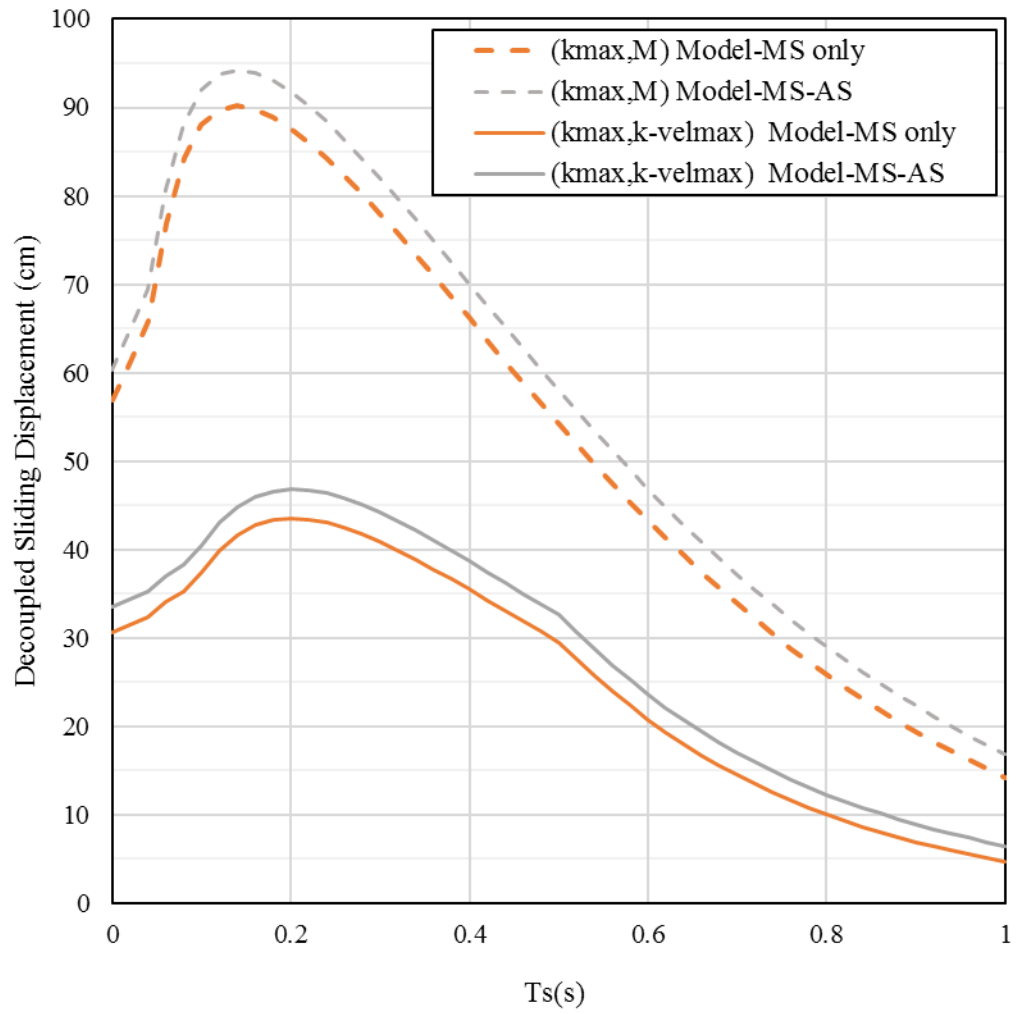


Figure 22: Decoupled Sliding displacements subjected to mainshock only and mainshock-aftershock sequence

Case Study

Two hypothetical 30-m slopes with average shear velocities of $V_s = 400$ m/s (Site B) and $V_s = 250$ m/s (Site C) were considered. The resulting site periods are 0.3 s for Site B and 0.48 s for Site C ($T_s = 4H/V_s$). The charts incorporated the effects of slope geometry, earthquake magnitude and yield acceleration as well as peak acceleration and predicted sliding displacements as a function of these quantities. Four seismic events with $M_w = 6.5, 7.0, 7.5,$ and 8 are considered. Commonly used ground motion prediction models are used to calculate PGA and PGV (Boore, et al. 2014) and T_m (Rathje, Wang, et al. 2014). For the T_m prediction, the closest distance from the epicenter to the site is assumed as 10 km. As summarized in Table 2 both PGA and PGV increase with the increase in earthquake magnitude.

Table 2: Summary of the predicted ground motion parameters [Rathje et al. (2014), Boore et al. (2014)]

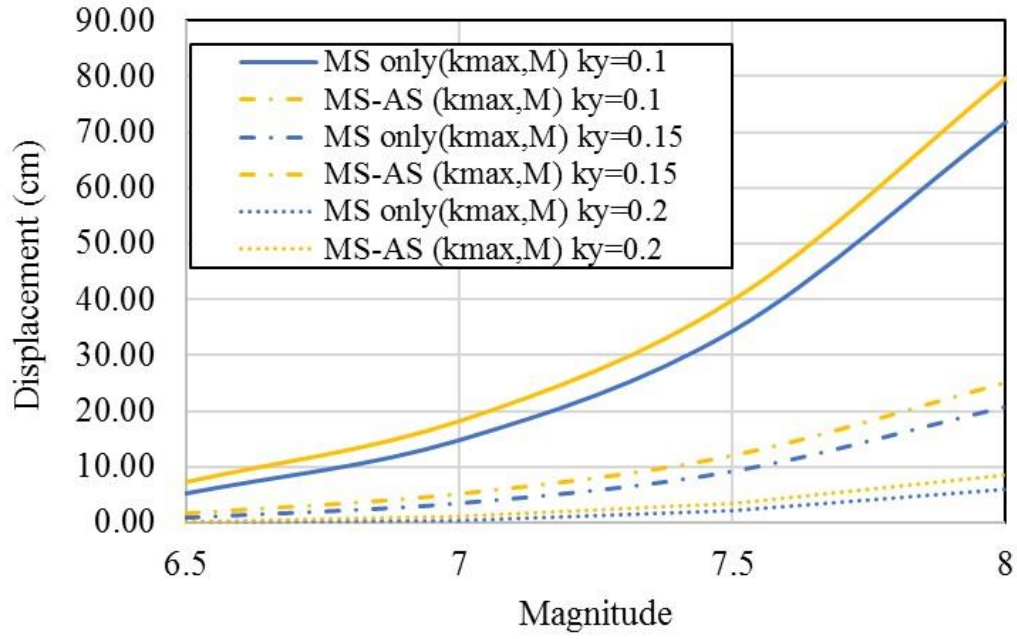
Site Class	Magnitude	PGA (g)	PGV (cm/s)	T_m (s)	T_s/T_m
Site B ($V_{s,30} = 400$ m/s)	6.5	0.27	26.54	0.51	0.59
	7.0	0.31	35.35	0.56	0.54
	7.5	0.36	47.05	0.58	0.52
	8	0.41	62.62	0.58	0.52
Site C ($V_{s,30} = 250$ m/s)	6.5	0.29	32.07	0.51	0.94
	7.0	0.32	41.92	0.56	0.86
	7.5	0.36	54.74	0.58	0.82
	8	0.40	71.40	0.58	0.82

Seismic loading parameters (k_{max} and $k\text{-vel}_{max}$) are calculated using the ground motion parameters and site characteristics summarized in Table 2 for a flexible slope with yield acceleration of 0.1 g. As summarized in Table 3, both sites experienced greater sliding displacement when subjected to mainshock – aftershock sequence compared to mainshock only case. On average, the increase in sliding displacement is around 30.9% for the scalar (k_{max}, M) model and 31.3% for the vector ($k_{max}, k\text{-vel}_{max}$) model.

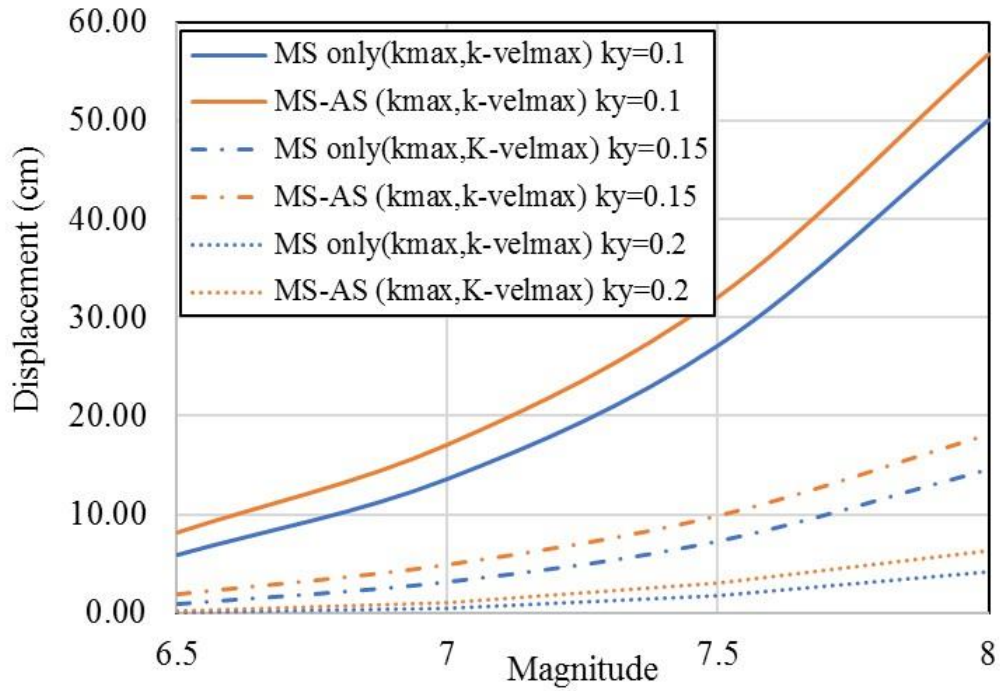
Table 3: Sliding displacements calculated with and without aftershocks for different site conditions for a slope with a $k_y=0.1$ g

Parameter	k_{\max} (g)	$k\text{-vel}_{\max}$ (cm/s)	Sliding displacement (k_{\max} , M) model (cm)		Sliding displacement (k_{\max} , $k\text{-vel}_{\max}$) model (cm)	
Seismic Environment	-	-	MS only	MS-AS	MS only	MS-AS
Corresponding Equation	Equation 1	Equation 2	Equation 3a	Equation 4a	Equation 3b	Equation 4b
Site B ($V_{s30}=400\text{m/s}$)	0.21	29.89	5.10	7.29	5.87	8.22
	0.25	39.60	14.68	18.34	13.60	17.13
	0.28	52.41	34.32	39.83	27.16	32.08
	0.31	69.16	71.86	79.73	50.06	56.67
Site C ($V_{s30}=250\text{m/s}$)	0.17	33.85	3.23	5.23	3.67	5.82
	0.20	44.40	9.21	12.92	8.56	12.11
	0.22	57.64	21.45	27.56	16.85	22.14
	0.23	74.04	42.92	52.10	29.30	36.64

Similar to the results presented in Table 3, Figure 23 shows the predictions of the sliding displacement models for mainshock only and mainshock-aftershock cases for site B at three yield accelerations ($k_y=0.1$ g, 0.15 g, and 0.2 g). In accordance with the previous observations, aftershocks increase seismic demands relative to the mainshock alone; thus, the seismic risk may be underestimated if aftershocks are neglected.



(a)



(b)

Figure 23: Sliding displacement predictions for mainshock only and mainshock-aftershock sequence as a function of earthquake magnitude using the (a) k_{\max}, M model and (b) $k_{\max}, k\text{-}vel_{\max}$ model (Site B)

Summary

This chapter presents the effects of aftershocks on post-mainshock “damaged” slopes. To investigate the impacts of strength degradation on the yield acceleration of post-mainshock slopes subjected to aftershocks, decoupled sliding displacements on post-mainshock slopes are predicted using different levels of damage cases (i.e. Δk_y). It is documented that the sliding displacements on post-mainshock slopes subjected to aftershocks increased on average around 30% at all site periods due to the combined effects of strength degradation and additional seismic demand by the aftershock. A case study is demonstrated to explain the effects of aftershocks on the seismic performance of post-mainshock flexible sliding masses. Overall, the results suggest that aftershocks increase the seismic demand relative to the mainshock alone; thus, the seismic risk is underestimated if aftershocks are neglected.

Chapter Six

Conclusions and Discussions

This thesis aims to provide an improved assessment of the risks associated with the seismic performance of slopes subjected to mainshock – aftershock sequences. Typically, aftershocks are smaller in magnitude; however, aftershock ground motion characteristics such as the intensity and duration can be greater than the mainshock due to the changes in the earthquake mechanism and location with respect to the site. After any earthquake, aftershocks typically continue over time with decreasing frequency and while not all aftershocks can exacerbate the damage from the mainshock, they can still significantly delay the recovery efforts. The same applies for the effects of aftershocks on earth slopes. Post-mainshock slopes may experience delayed failures due to undrained creep as there is not sufficient time for repair and retrofit between mainshock – aftershock sequences. Therefore, seismic stability analyses of earth slopes should account for mainshock – aftershock sequences. Seismic risks are underestimated if aftershocks are neglected.

Obtained from the PEER resources, a comprehensive dataset with strong ground motion records from a total of 144 mainshocks and their corresponding aftershocks were used in this study. As-recorded aftershocks were used in this research because a comparison of the resulting seismic demand parameters for earth slopes revealed that artificial aftershocks can lead to significant overestimation of the seismic demand parameters for earth slopes at relatively small displacement levels and unconservative estimation at relatively large displacement levels.

720 k-time histories with their corresponding seismic loading parameters (k_{\max} and $k\text{-vel}_{\max}$) were generated to incorporate the dynamic response of flexible slopes for

various site conditions. This dataset developed in this research includes a new subset of earthquake strong motion records from the PEER database. Hence, it is used to demonstrate that there is no dataset bias in the predictions of Rathje and Antonakos predictive models (2011).

In the literature, various empirical models are available that predict sliding displacement as a function of ground motion parameters and site parameters but the datasets for these empirical models do not include aftershock records. Thus, these empirical displacement predictive models do not perform well for slopes subjected to Mainshock - Aftershock sequences. As far as the author is concerned, the occurrence of aftershocks (i.e., multi-hazard approach) has not been included in the assessment of seismic performance of earth slopes. In the geotechnical earthquake engineering literature, there is a knowledge gap regarding the evaluation of the seismic performance of earth slopes subjected to multiple. This thesis aims to bridge this gap by incorporating aftershocks on the evaluation of the seismic performance of earth slopes. Using the k-time histories generated for various site conditions, decoupled sliding displacements were computed for mainshocks and aftershocks. The resulting decoupled sliding displacement dataset consisted of 968 non-zero sliding displacement values for mainshocks. Decoupled sliding displacements of post-mainshock slopes subjected to aftershocks were predicted by applying yield acceleration reduction factors to account for the strength degradation due to the mainshock. The resulting decoupled sliding displacement dataset consisted of 394 non-zero sliding displacement values for aftershocks. A comparison of the mainshock only and mainshock – aftershock cases suggested that decoupled sliding displacements on post-mainshock slopes subjected to aftershocks increased on average around 30% at all site periods. The original sliding

displacement predictive models for flexible slopes proposed by Rathje et al. (2014) are modified to incorporate the effects of aftershocks. These models predict the sliding displacement as a function of ground motion parameters and site parameters.

The failure of post- mainshock slopes is due to the combined effects of strength degradation and the additional seismic demand by aftershocks. Overall, the results suggested that aftershocks increase the seismic demand relative to the mainshock alone; thus, the seismic risks are underestimated if aftershocks are neglected. The risk assessment of earth slopes under post-mainshock conditions requires special attention and a systematic approach. This study presents a robust performance assessment that integrates the aftershock hazard with the mainshock hazard by including subsequent analyses following the mainshock (Multi-hazard approach). The results of this study can also lead to more robust, resilient, and sustainable design of different civil infrastructure. The overall benefits include extended service life of civil infrastructure and reduced social and economic disruption. This study contributes to the current knowledge base by enhancing the understanding about the consequences of aftershocks for the assessment of the seismic performance of earth slopes.

Future Recommendations:

The database developed in this study did not include strong aftershocks with magnitudes > 7.5 . The inclusion of strong aftershocks will definitely make the database more complete. The majority of the strong motion records were taken from the U.S. There is room for improvement in the database by adding earthquake strong motion data from various recording stations around the world. The outcome of this research is the sliding displacement prediction equations for flexible slopes subjected to aftershocks. These equations are required for the development of probabilistic methods

to evaluate the expected sliding displacement of earth slopes subjected to earthquake mainshock-aftershock sequences.

List of Symbols and Notations

MS: Mainshock

AS: Aftershock

PGA: Peak ground acceleration

PGV: Peak ground velocity

T_m : Mean period

T_s : Site period

I_a : Arias intensity

D_{5-95} : Duration of arias intensity from 5% to 95%

D_{5-75} : Duration of arias intensity from 5% to 95%

k_y : yield acceleration

k : Seismic loading parameter (vertically average acceleration)

k_{max} : maximum value of k-time history

$k\text{-vel}_{max}$: maximum value of k-vel time history

D : Sliding Displacement

$\ln D$: Sliding Displacement in lognormal terms

M : Magnitude

σ : Standard deviation

References

- Ambraseys, N. N., and M. J. Menu. 1988. "Earthquake-induced ground displacements." *Earthquake Engineering and Structural Dynamics*, Vol. 16 985-1006.
- Ambraseys, N. N., and M. Srbulov. 1994. "Attenuation of Earthquake-Induced Ground." *Earthquake Engineering and Structural Dynamics*, Vol. 23 467-487.
- Andersen, K. H. 2015. "Cyclic soil parameters for offshore foundation design." *Frontiers in Offshore Geotechnics III*.
- Antonakos, G. 2009. *Models of Dynamic Response and Decoupled Displacements of Earth Slopes during Earthquakes*. PhD Thesis, Austin, Tx: University of Texas at Austin.
- Antonakos, G., and E. M. Rathje. 2011. "A unified model for predicting earthquake-induced sliding displacements of rigid and." *Engineering Geology* 51-60.
- Arias, A. 1970. *Measure of Earthquake Intensity*. Massachusetts Institute of Technology, Cambridge University of Chile, Santiago de Chile.
- Bishop, A. W. 1955. "The use of the slip circle in the stability analysis of slopes." *Geotechnique*, 5 7-17.
- Boore, M.B., Stewart P.J., Seyhan E., and Atkinson M. G. 2014. "NGA-West 2 Equations for Predicting PGA, PGV, and 5% Damped PSA for Shallow Crustal Earthquakes." *Earthquake Spectra* 1057-1085.
- Bray, J. D. 2009. "Pseudostatic Coefficient for Use in Simplified Seismic Slope Stability Evaluation." *Journal of Geotechnical and Geoenvironmental Engineering* 1336-1340.

- Bray, J. D., and E. M. Rathje. 1998. "Earthquake-induced displacements of solid-waste landfills." *Journal of Geotechnical and Geoenvironmental Engineering, ASCE* 124 (3) 242–253.
- Bray, J.D., and T. Travarasou. 2007. "Simplified procedure for estimating earthquake-induced deviatoric slope displacements." *Journal of Geotechnical and Geoenvironmental Engineering* 381-392.
- Chiou, Brian, Bob Darragh, and Maury Power. 2005. *NGA Documentation*. Documentation, Nation Geospatial-Intelligence Agency (NGA).
- Duncan, J. M. 1996. "State of the art: Limit equilibrium and finite-element analysis of slopes." *Journal of Geotechnical Engineering* 0577-0596.
- Encyclopaedia Britannica. 2017. *Christchurch earthquakes of 2010-11*. October 12. Accessed March 09, 2019. <https://www.britannica.com/event/Christchurch-earthquakes-of-2010-2011>.
- . 2018. *Tangshan Earthquake of 1976*. July 18. Accessed March 09, 2019. <https://www.britannica.com/event/Tangshan-earthquake-of-1976>.
- Franklin, A. G., and F. K. Chang. 1977. *Earthquake Resistance of Earth and Rock-Fill Dams. Report 5. Permanent Displacements of Earth Embankments by Newmark Sliding Block Analysis*. Defense Technical Information Center.
- Fredlund, D.G., and J. Krahn. 1977. "Comparison of slope stability methods of analysis." *Can. Geotech J.*
- Goda, K. 2014. "Record selection for aftershock incremental dynamic analysis." *Earthquake Engineering and Structural Dynamics*.

- Han, R., Y. Li, and J. Lindt. 2014. "Seismic risk of base isolated non-ductile reinforced concrete buildings considering uncertainties and mainshock-aftershock sequences." *Structural Safety* 39-56.
- Hashash, Y. M. A., R. E. S. Moss, D. Asimaki, and K. B. Clahan. 2015. *Geotechnical Field Reconnaissance: Gorkha (Nepal) Earthquake of April 25 2015 and Related Shaking Sequence*. GEER Association.
- Hough, S. E, and M. T. Page. 2015. "A century of induced earthquakes in Oklahoma?" *Bulletin of the Seismological Society of America* (USGS).
- Janbu, N. 1954. "Applicaton of composite slip surface for stability analysis." *Europe Conference on Stability of Earth Slopes*. Sweden. 43-49.
- Jeon, J., R. DesRoches, L. N. Lowes, and I. Brilakis. 2015. "Framework of aftershock fragility assessment—case studies: older California reinforced concrete building frames." *Earthquake Engineering and Structural Dynamics*.
- Jibson, R. W., E. M. Rathje, M. W. Jibson, and Y. W. Lee. 2013. *Seismic Landslide Movement Modeled using Earthquake Records*. Software Manual, United States Department of the Interior, United States Geological Survey.
- Jibson, W. R., L. E. Harp, and A. J. Micheal. 2000. "A method for producing digital probabilistic seismic landslide hazard maps." *Engineering Geology* 271-289.
- Kim, C., C. Smell, and E. Medley. 2004. "Shear Strength of Franciscan Complex Melange as Calculated from Back-Analysis of a Landslide ." *Geotechnical Engineering Commons*. Missouri: Missouri University of Science and Technology Scholar's Mine.
- Kottke, A. R., and E. M. Rathje. 2009. *Technical Manual for Strata*. PEER Report 2008/10, California: Pacific Earthquake Engineering Reseach Center.

- Kramer, S. L. 1996. *Geotechnical Earthquake Engineering*. Prentice Hall Inc.
- Li, Y., R. Song, and J. W. Van De Lindt. 2014. "Collapse Fragility of Steel Structures Subjected to Earthquake Mainshock-Aftershock Sequences." *Journal of Structural Engineering* 140(12) Collapse Fragility of Steel Structures Subjected to Earthquake Mainshock-Aftershock Sequences.
- Lowe, J., and L. Karafiath. 1960. "Stability of Earth Dams Upon Drawdown." *Proceedings 1st Pan American Conference on Soil Mechanics and Foundation Engineering, Vol. 2*. Mexico City. 537-552.
- Makdisi, F.I., and H.B. Seed. 1978. "Simplified procedure for estimating dam and embankment earthquake-induced deformations." *ASCE Journal of the Geotechnical Engineering* 849-867.
- Margaris, B., C. Papaioannou, J. P. Stewart, and G. Athanasopoulos. 2008. *Preliminary Report on the Principal Seismological and Engineering Aspects of the Mw=6.5 Achaia-Ilia (Greece) Earthquake on 8 June 2008*. Los Angeles: GEER Association.
- Melo, C., and S. Sharma. 2004. "Seismic Coefficients for pseudostatic slope analysis." *13th World Conference on Earthquake Engineering*. Vancouver.
- Morgenstern, N., R., and V., E. Price. 1965. "The Analysis of the Stability of General Slip Surfaces. ." *Geotechnique, Vol. 15* 79-93.
- Newmark, N., M. 1965. "Effects of Earthquakes on Dams and Embankments." *Geotechnique, 15* 139-160.
2014. *PEER Ground Motion Database*. Accessed 2018.
<https://ngawest2.berkeley.edu/>.

- Raghunandan, M., A. B. Liel, and N. L. Luco. 2015. "Aftershock collapse vulnerability assessment of reinforced concrete." *Earthquake Engineering and Structural Dynamics* 419-439.
- Rathje, E. M, and G. Saygili. 2009. "Probabilistic assessment of earthquake-induced sliding displacements of natural slopes." *Bulletin of the New Zealand Society for Earthquake Engineering* 18-27.
- Rathje, E. M., and J. D. Bray. 2001. "One- and two-dimensional seismic analysis of solid-waste landfills." *Canadian Geotechnical Journal*, 38 850-862.
- Rathje, E. M., Y. Wang, P. J. Stafford, G. Antonakos, and G. Saygili. 2014. "Probabilistic assessment of the seismic performance of earth slopes." *Bulletin of Earthquake Engineering*, 12(3) 1071-1090.
- Rathje, E.M, Wang, Y., P.J. Stafford, G. Antonakos, and G. Saygili. 2014. "Probabilistic Assessment of th Seismic Performance of Earth Slopes." *Bulletin of Earthquake Engineering*, 12(3) 1071-1090.
- Rathje, Faraj, Russell, and Bray. 2004. "Empirical Relationships for Frequency Content Parameters of Earthquake Ground Motions ." *EERI Earthquake Spectra*.
- Ruiz-García, J., and J. C. Negrete-Manriquez. 2011. "Evaluation of drift demands in existing steel frames under as-recorded far-field and near-fault mainshock–aftershock seismic sequences." *Engineering Structures* 621-634.
- Ruiz-Gracia, J., and J.,D. Aguilar. 2017. "Influence of modeling assumptions and aftershock hazard level in seismic response of post-mainshock steel framed buildings." *Engineering Structures*, 140 437-446.
- SAS. 2018. "JMP." Computer Software.

- Saygili, G. 2008. "A probabilistic approach for evaluating earthquake induced landslides."
- Saygili, G., and E. M. Rathje. 2008. "Empirical Predictive Models for Earthquake Induced Sliding Displacement of Slopes." *Journal of Geotechnical and Geoenvironmental Engineering* 790-803.
- Saygili, G., and E. M. Rathje. Journal of Geotechnical Engineering. "Empirical Predictive Models for Earthquake Induced Sliding Displacement of Slopes."
- Skempton, A., W. 1985. "Residual strength of clays in landslides, folded strata and the laboratory." *Geotechnique* 3-18.
- Song, R., Y. Li, and J. W. Van de Lindt. 2014. "Impact of earthquake ground motion characteristics on collapse risk of post-mainshock buildings considering aftershocks." *Engineering Structures*.
- Spencer, E. 1967. "A method of analysis of the stability of embankments assuming parallel inter-slice forces." *Geotechnique*, 17 11-26.
- Strenk, P. M. 2010. *Evaluation of Analytical Procedures for Estimating Seismically Induced*. PhD Thesis, Drexel University.
- Sun, J., T. Hutchinson, K. Clahan, F. Menq, and E. Lo. 2016. *Geotechnical Reconnaissance of the 2016 Mw 6.3 Meinong Earthquake, Taiwan*. Geer Association.
- Tiwari, B., L., T. Brandon, H. Marui, and R., G. Tuladhar. 2005. "Comparison of Residual Shear Strengths from Back Analysis and Ring Shear Tests on Undisturbed and Remodeled Specimens." *Journal of Geotechnical and Geoenvironmental Engineering* 131(9) 1071-1079.

- U.S. Geological Survey . 2000. *Implications for Earthquake Risk Reduction in the United States from the Kocaeli, Turkey, Earthquake of August 17, 1999*.
United States Government Printing Office.
- n.d. *U.S. Geological Survey*. <https://www.usgs.gov/>.
- U.S. Geological Survey. n.d. *Foreshocks, aftershocks - what's the difference?*
Accessed 12 29, 2018. https://www.usgs.gov/faqs/foreshocks-aftershocks-whats-difference?qt-news_science_products=0#qt-news_science_products.
- US Army Corps of Engineers. 1968. *Engineering Design, Stability of Earth and Rockfill Dam, Revision Draft, February*. US Army Corps of Engineers.
- USGS. 2012. *M8.6- off the coast of Northern Sumatra* . April 11. Accessed March 09, 2019.
https://earthquake.usgs.gov/earthquakes/eventpage/official20120411083836720_20/executive.
- . 2015. *Magnitude 7.8 Earthquake in Nepal Aftershocks*. May 12. Accessed March 09, 2019. <https://www.usgs.gov/news/magnitude-78-earthquake-nepal-aftershocks>.
- . n.d. *The Science of Eathquakes*.
<https://earthquake.usgs.gov/learn/kids/eqscience.php>.
- Vrymoed, J. L., and E. R. Calzascia. 1978. "Simplified determination of dynamic stresses in earth dams." *Earthquake Engineering and Soil Dynamics*. New York: ASCE. 991-1006.
- Wang, Y. 2014. "Probabilistic assessments of the seismic stability of slopes: Improvements to site-specific and regional analyses." PhD Thesis.

- Watson-Lamprey, J., and N. Abrahamson. 2006. "Selection of Ground Motion Time Series and Limits on Scaling." *Soil Dynamics and Earthquake Engineering*, 26(5) 477-482.
- Whitman, R., V., and W., A. Bailey. 1967. "Use of computer for slope stability analysis." *ASCE Journal of the Soil Mechanics and Foundation Division*.
- Wikipedia. 2019. *1992 Landers Earthquake*. March 10. Accessed March 16, 2019. https://en.wikipedia.org/wiki/1992_Landers_earthquake#cite_ref-9.
- Wu, J., and P. Tsai. 2011. "New dynamic procedure for back-calculating the shear strength parameters of large landslides." *Engineering Geology* 123 129-147.
- Yegian, M. K., E. A. Marciano, and V. G. Ghahraman. 1991. "Earthquake-Induced Permanent Deformations: Probabilistic Approach." *Journal of Geotechnical Engineering*, Vol. 117, No. 1 35-50.
- Yin, Y., J., and Y. Li. 2010. "Seismic collapse risk of light-frame wood construction considering aleatoric and epistemic uncertainties." *Structural Safety* 32(4) 250-261.

Appendix A: Mainshocks

Earthquake Name	Motions	Date	Magnitude (M _w)	R _{closerst} (km)	V _{s30} (m/sec)	PGA (g)	PGV (cm/sec)	I _a (m/s)	T _m (sec)	D5-95 (sec)
Whittier Narrows	ALT000	10/1/1987	5.99	19.52	375.16	0.3	11	0.40	0.31	4
Whittier Narrows	ALT090	10/1/1987	5.99	19.52	375.16	0.2	5	0.19	0.24	8
Umbria Marche, Italy	AQP090	9/26/1997	6	83.48	298.73	0.0	1	0.00	0.98	56
Umbria Marche, Italy	AQP180	9/26/1997	6	83.48	298.73	0.0	1	0.00	0.89	50
Umbria Marche, Italy	AQG090	9/26/1997	6	83.48	298.73	0.0	1	0.00	1.06	57
Umbria Marche, Italy	AQG180	9/26/1997	6	83.48	298.73	0.0	1	0.00	0.99	49
Irpinia, Italy	BRZ000	11/23/1980	6.9	22.56	561.04	0.2	13	0.50	0.31	10
Irpinia, Italy	BRZ270	11/23/1980	6.9	22.56	561.04	0.2	10	0.41	0.33	13
Imperial Valley	CXO225	10/15/1979	6.53	10.45	231.23	0.3	22	0.86	0.44	11
Imperial Valley	CXO315	10/15/1979	6.53	10.45	231.23	0.2	19	0.75	0.42	15
Northridge	ANA090	1/17/1994	6.69	38	349.6	0.0	4	0.03	0.59	14
Northridge	ANA180	1/17/1994	6.69	38	349.6	0.1	5	0.09	0.51	15
Chi-Chi, Taiwan	CHY004-N	9/20/1999	7.62	47.32	271.3	0.1	15	0.33	0.38	68
Chi-Chi, Taiwan	CHY004-W	9/20/1999	7.62	47.32	271.3	0.1	21	0.40	0.87	76
Mammoth Lakes	CVK090	5/25/1980	6.06	6.63	382.12	0.4	24	2.24	0.33	9
Mammoth Lakes	CVK180	5/25/1980	6.06	6.63	382.12	0.4	24	2.60	0.24	10
Kocaeli, Turkey	DZC180	8/17/1999	7.51	15.37	281.86	0.3	59	1.09	0.99	12
Kocaeli, Turkey	DZC270	8/17/1999	7.51	15.37	281.86	0.4	56	1.33	0.87	11
Ancona, Italy	GEN000	1/25/1972	4	14.9	448.77	1.5	2	0.01	0.22	4
Ancona, Italy	GEN090	1/25/1972	4	14.9	448.77	0.1	2	0.01	0.17	3
Darfield, New Zealand	HVSCS26W	9/3/2010	7	24.47	422	0.6	42	3.83	0.28	14
Darfield, New Zealand	HVSCS64E	9/3/2010	7	24.47	422	0.6	23	4.12	0.23	16
Hollister	HCH181	4/9/1961	5.6	19.56	198.77	0.1	8	0.13	0.67	19
Hollister	HCH271	4/9/1961	5.6	19.56	198.77	0.1	10	0.20	0.71	17
Imperial Valley	HVP225	10/15/1979	6.53	7.5	202.89	0.3	53	0.89	0.62	12
Imperial Valley	HVP315	10/15/1979	6.53	7.5	202.89	0.2	51	0.86	0.71	13
Northwest China	JIA000	4/5/1997	5.9	24.06	240.09	0.3	7	0.49	0.22	14
Northwest China	JIA270	4/5/1997	5.9	24.06	240.09	0.2	16	0.61	0.34	10
Kalamata, Greece	KAL-NS	9/13/1986	6.2	6.45	382.21	0.2	34	0.55	0.59	5
Kalamata, Greece	KAL-WE	9/13/1986	6.2	6.45	382.21	0.3	23	0.73	0.52	6
Northridge	PEL090	1/17/1994	6.69	24.03	316.46	0.2	18	0.94	0.48	12
Northridge	PEL360	1/17/1994	6.69	24.03	316.46	0.4	27	2.00	0.37	11
Molise, Italy	ASE000	1/11/2002	5.7	130.9	547	0.0	0	0.00	0.40	34
Molise, Italy	ASE270	1/11/2002	5.7	130.9	547	0.0	0	0.00	0.39	33
L'Aquila, Italy	GX066XTE	4/6/2009	6.3	6.27	475	0.7	40	2.84	0.33	8
L'Aquila, Italy	GX066YLN	4/6/2009	6.3	6.27	475	0.6	43	2.00	0.34	8
L'Aquila, Italy	FA030XTE	4/6/2004	6.3	6.81	685	0.5	31	1.38	0.45	8

Earthquake Name	Motions	Date	Magnitude (M _w)	R _{closerst} (km)	V _{s30} (m/sec)	PGA (g)	PGV (cm/sec)	I _a (m/s)	T _m (sec)	D5-95 (sec)
L'Aquila, Italy	FA030YLN	4/6/2004	6.3	6.81	685	0.5	36	1.37	0.44	8
Mammoth Lakes	MLS254	5/25/1980	6.06	4.67	346.82	0.3	16	0.69	0.27	8
Mammoth Lakes	MLS344	5/25/1980	6.06	4.67	346.82	0.2	16	0.80	0.26	8
Managua, Nicaragua	ESO090	12/23/1972	6.24	4.06	288.77	0.4	29	1.57	0.46	11
Managua, Nicaragua	ESO180	12/23/1972	6.24	4.06	288.77	0.3	31	2.01	0.41	8
Chalfant Valley	BPL070	7/20/1986	5.77	15.13	585.12	0.0	3	0.02	0.39	17
Chalfant Valley	BPL160	7/20/1986	5.77	15.13	585.12	0.1	9	0.04	0.38	9
Livermore	KOD180	1/24/1980	5.8	17.24	377.51	0.1	21	0.21	1.00	10
Livermore	KOD270	1/24/1980	5.8	17.24	377.51	0.1	8	0.08	0.61	14
Whittier Narrows	OBR270	10/1/1987	5.99	15.18	349.43	0.4	14	1.05	0.27	8
Whittier Narrows	OBR360	10/1/1987	5.99	15.18	349.43	0.4	22	1.27	0.26	7
Coalinga	PVY045	5/2/1983	6.36	8.41	257.38	0.6	61	4.13	0.56	8
Coalinga	PVY135	5/2/1983	6.36	8.41	257.38	0.5	39	3.83	0.39	9
Chi-Chi, Taiwan	CHY008-N	9/20/1999	7.62	40.43	210.73	0.1	23	0.45	1.17	58
Chi-Chi, Taiwan	CHY008-W	9/20/1999	7.62	40.43	210.73	0.1	31	0.52	1.19	52
Chalfant Valley	SHE009	7/20/1986	5.77	24.45	456.83	0.1	2	0.02	0.32	15
Chalfant Valley	SHE099	7/20/1986	5.77	24.45	456.83	0.0	2	0.01	0.38	17
Darfield, New Zealand	KPOCN15E	9/23/2010	7	30.53	255	0.4	40	1.49	0.61	20
Darfield, New Zealand	KPOCS75E	9/23/2010	7	30.53	255	0.3	33	1.60	0.53	17
Irpinia, Italy	TRC000	11/23/1980	6.9	53.16	496.46	0.0	6	0.03	0.68	23
Irpinia, Italy	TRC270	11/23/1980	6.9	53.16	496.46	0.0	6	0.04	0.95	21
Kocaeli, Turkey	KUT090	8/17/1999	7.51	145.06	399.61	0.1	16	0.21	1.42	57
Kocaeli, Turkey	KUT180	8/17/1999	7.51	145.06	399.61	0.1	9	0.14	1.34	53
Livermore	FRE075	1/24/1980	5.8	35.68	367.57	0.0	4	0.02	0.65	10
Livermore	FRE345	1/24/1980	5.8	35.68	367.57	0.1	4	0.03	0.73	10
Gulf of California	CXO090	12/8/2001	5.7	85.56	231.23	0.0	2	0.01	0.87	57
Gulf of California	CXO360	12/8/2001	5.7	85.56	231.23	0.0	2	0.01	0.89	51
Gulf of California	CAL090	12/8/2001	5.7	130.07	205.78	0.0	1	0.00	0.61	35
Gulf of California	CAL360	12/8/2001	5.7	130.07	205.78	0.0	1	0.00	0.66	37
Whittier Narrows	ALH180	10/1/1987	5.99	14.66	549.75	0.3	22	0.81	0.39	5
Whittier Narrows	ALH270	10/1/1987	5.99	14.66	549.75	0.4	17	0.87	0.29	6
Imperial Valley	DLT262	10/15/1979	6.53	22.03	242.05	0.2	26	2.39	0.63	51
Imperial Valley	DLT352	10/15/1979	6.53	22.03	242.05	0.3	33	3.28	0.69	51
Northridge	ORR090	1/17/1994	6.69	20.72	450.28	0.6	52	2.79	0.54	9
Northridge	ORR360	1/17/1994	6.69	20.72	450.28	0.5	52	3.16	0.69	9
Chalfant Valley	BEN270	7/20/1986	5.77	24.33	370.94	0.1	3	0.04	0.36	18
Chalfant Valley	BEN360	7/20/1986	5.77	24.33	370.94	0.1	3	0.03	0.33	17
Livermore	A3E146	1/24/1980	5.8	30.59	517.06	0.1	4	0.03	0.38	9
Livermore	A3E236	1/24/1980	5.8	30.59	517.06	0.1	3	0.04	0.33	10
Whittier Narrows	OLD000	10/1/1987	5.99	19.17	397.27	0.2	10	0.43	0.28	5
Whittier Narrows	OLD090	10/1/1987	5.99	19.17	397.27	0.3	9	0.29	0.28	7

Earthquake Name	Motions	Date	Magnitude (M _w)	R _{closerst} (km)	V _{s30} (m/sec)	PGA (g)	PGV (cm/sec)	I _a (m/s)	T _m (sec)	D5-95 (sec)
Imperial Valley	E01140	10/15/1979	6.53	21.68	237.33	0.1	16	0.29	0.36	15
Imperial Valley	E01230	10/15/1979	6.53	21.68	237.33	0.1	11	0.22	0.34	20
Northridge	H12090	1/17/1994	6.69	21.36	602.1	0.2	12	0.33	0.25	10
Northridge	H12180	1/17/1994	6.69	21.36	602.1	0.3	9	0.47	0.22	10
Chalfant Valley	LAD180	7/20/1986	5.77	23.47	303.47	0.1	10	0.12	0.85	21
Chalfant Valley	LAD270	7/20/1986	5.77	23.47	303.47	0.1	6	0.09	0.77	22
Livermore	SRM070	1/24/1980	5.8	17.93	384.47	0.1	3	0.04	0.60	25
Livermore	SRM340	1/24/1980	5.8	17.93	384.47	0.0	4	0.05	0.74	27
Gulf of California	2027A090	12/8/2001	5.7	96.28	276.25	0.0	1	0.00	0.76	64
Gulf of California	2027B360	12/8/2001	5.7	96.28	276.25	0.0	1	0.00	0.81	65
Whittier Narrows	WON075	10/1/1987	5.99	27.64	1222.52	0.0	2	0.01	0.20	7
Whittier Narrows	WON165	10/1/1987	5.99	27.64	1222.52	0.0	2	0.01	0.25	7
Imperial Valley	BCR140	10/15/1979	6.53	2.66	223.03	0.6	47	3.99	0.48	10
Imperial Valley	BCR230	10/15/1979	6.53	2.66	223.03	0.8	45	6.06	0.46	10
Northridge	ELL090	1/17/1994	6.69	36.55	326.19	0.2	7	0.24	0.41	10
Northridge	ELL180	1/17/1994	6.69	36.55	326.19	0.1	9	0.24	0.41	12
Irpinia, Italy	BAG000	11/23/1980	6.9	8.18	649.67	0.1	24	0.33	0.68	20
Irpinia, Italy	BAG270	11/23/1980	6.9	8.18	649.67	0.2	35	0.43	0.99	16
L'Aquila, Italy	BS029XTE	4/6/2009	6.3	89.89	630	0.0	2	0.00	0.81	26
L'Aquila, Italy	BS029YLN	4/6/2009	6.3	89.89	630	0.0	1	0.00	0.64	28
Chi-Chi, Taiwan	CHY042-E	9/20/1999	7.62	28.17	665.2	0.1	15	0.32	0.87	31
Chi-Chi, Taiwan	CHY042-N	9/20/1999	7.62	28.17	665.2	0.1	11	0.15	0.73	37
Kocaeli, Turkey	YPT060	8/17/1999	7.51	4.83	297	0.2	70	1.33	1.24	15
Kocaeli, Turkey	YPT150	8/17/1999	7.51	4.83	297	0.3	72	1.32	1.34	15
Kocaeli, Turkey	ARE000	8/17/1999	7.51	13.49	523	0.2	14	0.29	0.31	11
Kocaeli, Turkey	ARE090	8/17/1999	7.51	13.49	523	0.1	40	0.22	0.60	10
Northwest China	XIK000	4/5/1997	5.9	52.36	341.56	0.0	3	0.03	0.27	20
Northwest China	XIK270	4/5/1997	5.9	52.36	341.56	0.0	2	0.04	0.24	20
Darfield, New Zealand	FGPSN02E	9/3/2010	7	141.18	476.62	0.0	6	0.02	1.11	40
Darfield, New Zealand	FGPSN88W	9/3/2010	7	141.18	476.62	0.0	5	0.02	1.05	37
Darfield, New Zealand	HPSCN04W	9/3/2010	7	25.4	206	0.1	24	0.62	0.97	16
Darfield, New Zealand	HPSCS86W	9/3/2010	7	25.4	206	0.1	28	0.42	1.14	26
Chi-Chi, Taiwan	CHY014-N	9/20/1999	7.62	34.18	347.63	0.3	23	1.69	0.55	27
Chi-Chi, Taiwan	CHY014-W	9/20/1999	7.62	34.18	347.63	0.2	24	1.68	0.55	26
Umbria Marche, Italy	BEV000	9/26/1997	6	18.86	401.34	0.1	7	0.15	0.61	21
Umbria Marche, Italy	BEV270	9/26/1997	6	18.86	401.34	0.1	9	0.19	0.65	20
Umbria Marche, Italy	CLF000	9/26/1997	6	6.92	317	0.2	18	0.47	0.61	9
Umbria Marche, Italy	CLF270	9/26/1997	6	6.92	317	0.2	13	0.40	0.54	11
Irpinia, Italy	BOV000	11/23/1980	6.9	46.25	356.39	0.0	4	0.04	0.44	28
Irpinia, Italy	BOV270	11/23/1980	6.9	46.25	356.39	0.0	3	0.05	0.38	26
L'Aquila, Italy	BY003XTE	4/6/2009	6.3	35.44	415.23	0.0	2	0.01	0.65	22

Earthquake Name	Motions	Date	Magnitude (M _w)	R _{closest} (km)	V _{s30} (m/sec)	PGA (g)	PGV (cm/sec)	I _a (m/s)	T _m (sec)	D5-95 (sec)
L'Aquila, Italy	BY003YLN	4/6/2009	6.3	35.44	415.23	0.0	1	0.01	0.63	24
L'Aquila, Italy	AV122XTE	4/6/2009	6.3	172.15	574.88	0.0	0	0.00	0.88	54
L'Aquila, Italy	AV122XLN	4/6/2009	6.3	172.15	574.88	0.0	0	0.00	0.94	53
Molise, Italy	CMM000	1/11/2002	5.7	34.29	519	0.0	0	0.00	0.69	50
Molise, Italy	CMM270	1/11/2002	5.7	34.29	519	0.0	1	0.00	0.78	47
Molise, Italy	ORT000	1/11/2002	5.7	97.51	388.01	0.0	0	0.00	0.47	23
Molise, Italy	ORT270	1/11/2002	5.7	97.51	388.01	0.0	0	0.00	0.41	24
Molise, Italy	CHT000	1/11/2002	5.7	90.94	356.39	0.0	0	0.00	0.30	31
Molise, Italy	CHT270	1/11/2002	5.7	90.94	356.39	0.0	0	0.00	0.31	30
Gulf of California	E11090	12/8/2001	5.7	98.65	196.25	0.0	2	0.01	0.89	55
Gulf of California	E11360	12/8/2001	5.7	98.65	196.25	0.0	2	0.01	0.82	57
Chi-Chi, Taiwan	CHY012-N	9/20/1999	7.62	59.04	198.4	0.1	17	0.24	1.38	82
Chi-Chi, Taiwan	CHY012-W	9/20/1999	7.62	59.04	198.4	0.1	12	0.25	1.33	80
Chalfant Valley	ZAK270	7/20/1986	5.77	6.39	316.19	0.3	24	0.53	0.42	8
Chalfant Valley	ZAK360	7/20/1986	5.77	6.39	316.19	0.2	24	0.54	0.45	11
Irpinia, Italy	BIS000	11/23/1980	6.9	21.26	496.46	0.1	23	0.19	1.19	24
Irpinia, Italy	BIS270	11/23/1980	6.9	21.26	496.46	0.1	14	0.15	1.12	27
Umbria Marche, Italy	NCR000	9/26/1997	6	8.92	428	0.5	33	2.48	0.24	5
Umbria Marche, Italy	NCR270	9/26/1997	6	8.92	428	0.4	28	2.37	0.30	4
Kocaeli, Turkey	DHM180	8/17/1999	7.51	60.05	354.37	0.1	25	0.20	0.99	35
Kocaeli, Turkey	DHM090	8/17/1999	7.51	60.05	354.37	0.1	16	0.15	0.87	37
Darfield, New Zealand	CACSN40E	9/3/2010	7	14.48	280.26	0.2	34	0.74	0.58	31
Darfield, New Zealand	CACSN50W	9/3/2010	7	14.48	280.26	0.2	47	0.86	0.68	35
Gulf of California	E07090	12/8/2001	5.7	100.55	210.51	0.0	1	0.00	0.63	57
Gulf of California	E07360	12/8/2001	5.7	100.55	210.51	0.0	1	0.00	0.68	57

Appendix B: Aftershocks

Earthquake Name	Motions	Date	Magnitude (M _w)	R _{closest} (km)	V _{s30} (m/sec)	PGA (g)	PGV (cm/sec)	I _a (m/s)	T _m (sec)	D5-95 (sec)
Whittier Narrows	ALT000	10/4/1987	5.27	15.38	375.16	0.27	12.5	0.19	0.23	2
Whittier Narrows	ALT090	10/4/1987	5.27	15.38	375.16	0.20	9.7	0.14	0.24	3
Umbria Marche, Italy	AQP090	10/6/1997	5.5	86.37	298.73	0.00	0.4	0.00	1.04	32
Umbria Marche, Italy	AQP180	10/6/1997	5.5	86.37	298.73	0.00	0.5	0.00	0.95	28
Umbria Marche, Italy	AQG090	10/6/1997	5.5	86.37	298.73	0.00	0.4	0.00	1.14	31
Umbria Marche, Italy	AQG180	10/6/1997	5.5	86.37	298.73	0.00	0.4	0.00	1.12	33
Irpinia, Italy	BRZ000	11/23/1980	6.2	42.65	561.04	0.04	3.5	0.03	0.55	22
Irpinia, Italy	BRZ270	11/23/1980	6.2	42.65	561.04	0.04	3.1	0.03	0.54	19
Imperial Valley	CXO225	10/15/1979	5.01	13.32	231.23	0.10	8.1	0.04	0.48	9
Imperial Valley	CXO315	10/15/1979	5.01	13.32	231.23	0.07	5.6	0.03	0.39	12
Northridge-02	ANA090	1/17/1994	6.05	38.14	349.6	0.01	0.4	0.00	0.26	15
Northridge-02	ANA180	1/17/1994	6.05	38.14	349.6	0.01	0.5	0.00	0.23	15
Chi-Chi, Taiwan	CHY004N	9/20/1999	5.9	86.14	271.3	0.04	1.7	0.01	0.40	19
Chi-Chi, Taiwan	CHY004W	9/20/1999	5.9	86.14	271.3	0.03	1.3	0.01	0.31	19
Mammoth Lakes	CVK090	5/25/1980	5.69	9.46	382.12	0.16	11.6	0.24	0.44	7
Mammoth Lakes	CVK180	5/25/1980	5.69	9.46	382.12	0.18	13.2	0.20	0.44	8
Duzce, Turkey	DZC180	11/12/1999	7.14	6.58	281.86	0.40	71.2	2.70	0.71	11
Duzce, Turkey	DZC270	11/12/1999	7.14	6.58	281.86	0.51	84.2	2.93	0.82	11
Ancona, Italy	GEN000	2/4/1972	4.6	7.3	448.77	0.12	2.8	0.07	0.20	4
Ancona, Italy	GEN090	2/4/1972	4.6	7.3	448.77	0.12	4.5	0.11	0.18	3
Christchurch, New Zealand	HVSCS26W	2/21/2011	6.2	3.36	422	1.65	100.8	12.40	0.39	5
Christchurch, New Zealand	HVSCS64E	2/21/2011	6.2	3.36	422	1.29	61.1	11.37	0.34	6
Hollister	HCH181	4/9/1961	5.5	18.08	198.77	0.06	5.8	0.08	0.63	16
Hollister	HCH271	4/9/1961	5.5	18.08	198.77	0.07	9.3	0.10	0.74	15
Imperial Valley	HVP225	10/15/1979	5.01	10.58	202.89	0.11	7.3	0.06	0.29	7
Imperial Valley	HVP315	10/15/1979	5.01	10.58	202.89	0.25	16.2	0.13	0.58	6
Northwest China	JIA000	4/6/1997	5.93	37.26	240.09	0.12	10.9	0.19	0.33	18
Northwest China	JIA0270	4/6/1997	5.93	37.26	240.09	0.14	10.9	0.21	0.31	16
Kalamata, Greece	KAL-NS	9/15/1986	5.4	5.6	382.21	0.24	22.1	0.28	0.51	3
Kalamata, Greece	KAL-WE	9/15/1986	5.4	5.6	382.21	0.14	7.8	0.08	0.45	4
Northridge	PEL090	17-Jan	6.05	20.68	316.46	0.158	3.37536	0.05	0.188	3.48
Northridge	PEL360	17-Jan	6.05	20.68	316.46	0.17	6.9	0.06	0.23	4
Molise, Italy	ASE000	10/31/2002	5.7	138.3	547	0.00	0.1	0.00	0.85	62
Molise, Italy	ASE270	10/31/2002	5.7	138.3	547	0.00	0.1	0.00	0.99	71
L'Aquila, Italy	GX333XTE	4/7/2009	5.6	14.81	475	0.13	5.2	0.12	0.25	5
L'Aquila, Italy	GX333YLN	4/7/2009	5.6	14.81	475	0.15	5.4	0.13	0.26	4
L'Aquila, Italy	FA194XTE	4/7/2004	5.6	14.95	685	0.15	6.3	0.10	0.32	5
L'Aquila, Italy	FA194YLN	4/7/2004	5.6	14.95	685	0.11	6.3	0.09	0.30	6
Mammoth Lakes	MLS254	5/25/1980	5.69	9.12	346.82	0.39	24.2	0.63	0.23	4
Mammoth Lakes	MLS344	5/25/1980	5.69	9.12	346.82	0.44	24.0	1.26	0.22	3
Managua, Nicaragua	ESO090	12/23/1972	5.2	4.98	288.77	0.26	25.4	0.43	0.61	8
Managua, Nicaragua	ESO180	12/23/1972	5.2	4.98	288.77	0.22	17.9	0.35	0.40	8
Chalfant Valley	BPL070	7/21/1986	6.19	18.31	585.12	0.17	5.5	0.13	0.23	11
Chalfant Valley	BPL160	7/21/1986	6.19	18.31	585.12	0.16	12.7	0.20	0.30	9
Livermore	KOD180	1/27/1980	5.42	18.28	377.51	0.28	23.0	0.25	0.59	6

Earthquake Name	Motions	Date	Magnitude (M _w)	R _{closest} (km)	V _{s30} (m/sec)	PGA (g)	PGV (cm/sec)	I _a (m/s)	T _m (sec)	D5-95 (sec)
Livermore	KOD270	1/27/1980	5.42	18.28	377.51	0.08	6.5	0.06	0.53	12
Whittier Narrows	OBR270	10/4/1987	5.27	13.62	349.43	0.34	14.3	0.44	0.24	5
Whittier Narrows	OBR360	10/4/1987	5.27	13.62	349.43	0.32	18.0	0.40	0.34	6
Coalinga	PVY045	5/9/1983	5.09	12.4	257.38	0.10	8.6	0.04	0.45	5
Coalinga	PVY135	5/9/1983	5.09	12.4	257.38	0.21	9.9	0.10	0.28	2
Chi-Chi, Taiwan	CHY008N	9/20/1999	5.9	83.22	210.73	0.02	1.3	0.01	0.40	25
Chi-Chi, Taiwan	CHY008W	9/20/1999	5.9	83.22	210.73	0.03	1.3	0.01	0.31	19
Chalfant Valley	CHY042	7/21/1986	6.19	24.47	456.83	0.16	7.2	0.13	0.31	9
Chalfant Valley	CHY042	7/21/1986	6.19	24.47	456.83	0.09	5.6	0.09	0.38	10
Christchurch, New Zealand	KPOCN15E	2/21/2011	6.2	17.87	255	0.19	22.4	0.51	0.52	9
Christchurch, New Zealand	KPOCS75E	2/21/2011	6.2	17.87	255	0.22	15.0	0.66	0.48	12
Irpinia, Italy	TRC000	11/23/1980	6.2	64.37	496.46	0.02	3.3	0.01	0.94	19
Irpinia, Italy	TRC270	11/23/1980	6.2	64.37	496.46	0.02	4.2	0.01	0.99	22
Duzce, Turkey	KUT090	11/12/1999	7.14	168.3	399.61	0.02	9.8	0.04	2.56	43
Duzce, Turkey	KUT180	11/12/1999	7.14	168.3	399.61	0.02	5.0	0.02	1.71	55
Livermore	FRE075	1/27/1980	5.42	28.44	367.57	0.04	4.6	0.01	0.70	7
Livermore	FRE345	1/27/1980	5.42	28.44	367.57	0.04	3.3	0.01	0.66	9
CA/Baja Border Area	CXO090	2/22/2002	5.31	39.95	231.23	0.08	3.3	0.05	0.48	41
CA/Baja Border Area	CXO360	2/22/2002	5.31	39.95	231.23	0.11	5.1	0.04	0.44	40
CA/Baja Border Area	CAL090	2/22/2002	5.31	89.34	205.78	0.01	1.0	0.00	0.85	74
CA/Baja Border Area	CAL360	2/22/2002	5.31	89.34	205.78	0.01	1.4	0.00	0.85	77
Whittier Narrows	ALH180	10/4/1987	5.27	12.01	549.75	0.18	10.8	0.16	0.31	4
Whittier Narrows	ALH270	10/4/1987	5.27	12.01	549.75	0.21	9.0	0.12	0.34	8
Imperial Valley	DLT262	10/15/1979	5.01	49.93	242.05	0.06	1.9	0.02	0.21	12
Imperial Valley	DLT352	10/15/1979	5.01	49.93	242.05	0.12	3.6	0.04	0.25	11
Northridge	ORR090	1/17/1994	6.05	29.54	450.28	0.03	1.3	0.01	0.30	12
Northridge	ORR360	1/17/1994	6.05	29.54	450.28	0.02	0.9	0.00	0.33	15
Chalfant Valley	BEN270	7/21/1986	6.19	21.92	370.94	0.21	13.7	0.36	0.54	17
Chalfant Valley	BEN360	7/21/1986	6.19	21.92	370.94	0.18	15.9	0.32	0.60	13
Livermore	A3E146	1/27/1980	5.4	30	517.06	0.06	4.0	0.01	0.54	7
Livermore	A3E236	1/27/1980	5.4	30	517.06	0.03	1.4	0.01	0.34	11
Whittier Narrows	OLD000	10/4/1987	5.27	14.82	397.27	0.37	13.3	0.35	0.21	1
Whittier Narrows	OLD090	10/4/1987	5.27	14.82	397.27	0.44	14.8	0.24	0.24	2
Imperial Valley	E01140	10/15/1979	5.01	24.84	237.33	0.06	5.0	0.02	0.42	5
Imperial Valley	E01230	10/15/1979	5.01	24.84	237.33	0.03	0.9	0.00	0.21	5
Northridge	H12090	1/17/1994	6.05	28.21	602.1	0.01	0.3	0.00	0.16	15
Northridge	H12180	1/17/1994	6.05	28.21	602.1	0.02	0.4	0.00	0.14	12
Chalfant Valley	LAD180	7/21/1986	6.19	17.17	303.47	0.25	19.6	0.50	0.59	13
Chalfant Valley	LAD270	7/21/1986	6.19	17.17	303.47	0.18	19.5	0.39	0.58	17
Livermore	SRM070	1/27/1980	5.4	22.22	384.47	0.05	3.9	0.03	0.53	19
Livermore	SRM340	1/27/1980	5.4	22.22	384.47	0.05	4.1	0.04	0.56	17
CA/Baja Border Area	207A090	2/22/2002	5.31	53.08	276.25	0.06	2.6	0.03	0.44	51
CA/Baja Border Area	207B360	2/22/2002	5.31	53.08	276.25	0.06	2.5	0.03	0.44	50
Whittier Narrows	WON075	10/4/1987	5.27	28.42	1222.52	0.02	0.6	0.00	0.19	7
Whittier Narrows	WON165	10/4/1987	5.27	28.42	1222.52	0.02	0.6	0.00	0.19	6
Imperial Valley	BCR140	10/15/1979	5.01	13.04	223.03	0.07	3.8	0.02	0.36	12
Imperial Valley	BCR230	10/15/1979	5.01	13.04	223.03	0.13	8.1	0.04	0.59	10

Earthquake Name	Motions	Date	Magnitude (M _w)	R _{closest} (km)	V _{s30} (m/sec)	PGA (g)	PGV (cm/sec)	I _a (m/s)	T _m (sec)	D5-95 (sec)
Northridge	ELL090	1/17/1994	6.05	39.58	326.19	0.02	0.7	0.00	0.31	17
Northridge	ELL180	1/17/1994	6.05	39.58	326.19	0.02	0.6	0.00	0.25	17
Irpinia, Italy	BAG000	11/23/1980	6.2	19.56	649.67	0.06	4.0	0.03	0.54	14
Irpinia, Italy	BAG270	11/23/1980	6.2	19.56	649.67	0.05	4.4	0.02	0.67	22
L'Aquila, Italy	BS030XTE	4/7/2009	5.6	91.56	630	0.00	0.2	0.00	0.46	27
L'Aquila, Italy	BS030YLN	4/7/2009	5.6	91.56	630	0.00	0.3	0.00	0.43	25
Chi-Chi, Taiwan	CHY042E	9/20/1999	5.9	70.33	665.2	0.01	0.7	0.00	0.41	20
Chi-Chi, Taiwan	CHY042N	9/20/1999	5.9	70.33	665.2	0.01	0.6	0.00	0.39	18
Duzce, Turkey	YPT060	11/12/1999	7.14	97.53	297	0.02	3.7	0.01	0.85	42
Duzce, Turkey	YPT150	11/12/1999	7.14	97.53	297	0.02	8.7	0.02	0.99	37
Duzce, Turkey	ARE000	11/12/1999	7.14	131.5	523	0.01	2.7	0.00	0.80	32
Duzce, Turkey	ARE090	11/12/1999	7.14	131.5	523	0.01	2.8	0.00	0.92	27
Northwest China-02	XIK000	4/6/1997	5.93	46.24	341.56	0.07	2.6	0.06	0.28	21
Northwest China-02	XIK270	4/6/1997	5.93	46.24	341.56	0.07	3.3	0.07	0.26	23
Christchurch, New Zealand	FGPSN02E	2/21/2011	6.2	214.8	476.62	0.00	0.7	0.00	0.85	36
Christchurch, New Zealand	FGPSN88W	2/21/2011	6.2	214.8	476.62	0.00	0.8	0.00	0.79	38
Christchurch, New Zealand	HPSCN04W	2/21/2011	6.2	4.35	206	0.21	26.9	0.32	0.98	11
Christchurch, New Zealand	HPSCS86W	2/21/2011	6.2	4.35	206	0.27	49.1	0.85	0.96	10
Chi-Chi, Taiwan	CHY014N	9/20/1999	5.9	76.23	347.63	0.02	1.2	0.01	0.39	16
Chi-Chi, Taiwan	CHY014W	9/20/1999	5.9	76.23	347.63	0.02	1.3	0.01	0.40	17
Umbria Marche, Italy	BEV000	10/6/1997	5.5	17.08	401.34	0.04	3.3	0.03	0.55	18
Umbria Marche, Italy	BEV270	10/6/1997	5.5	17.08	401.34	0.05	4.8	0.05	0.65	19
Umbria Marche, Italy	CLF000	10/6/1997	5.5	7.91	317	0.13	11.4	0.12	0.66	8
Umbria Marche, Italy	CLF270	10/6/1997	5.5	7.91	317	0.11	10.0	0.10	0.60	7
Irpinia, Italy	BOV000	11/23/1980	6.2	43.5	356.39	0.03	2.9	0.01	0.48	15
Irpinia, Italy	BOV270	11/23/1980	6.2	43.5	356.39	0.03	2.2	0.01	0.47	16
L'Aquila, Italy	BY008XTE	4/7/2009	5.6	37.99	415.23	0.01	0.8	0.00	0.52	20
L'Aquila, Italy	BY008YLN	4/7/2009	5.6	37.99	415.23	0.00	0.4	0.00	0.53	24
L'Aquila, Italy	AV123XTE	4/7/2009	5.6	186	574.88	0.00	0.2	0.00	0.82	45
L'Aquila, Italy	AV123YLN	4/7/2009	5.6	186	574.88	0.00	0.2	0.00	0.70	50
Molise, Italy	CMM000	10/31/2002	5.7	42.81	519	0.01	0.6	0.00	0.71	48
Molise, Italy	CMM270	10/31/2002	5.7	42.81	519	0.01	0.9	0.00	0.66	47
Molise, Italy	ORT000	10/31/2002	5.7	107.5	388.01	0.00	0.5	0.00	0.52	20
Molise, Italy	ORT270	10/31/2002	5.7	107.5	388.01	0.00	0.3	0.00	0.46	28
Molise, Italy	CHT000	10/31/2002	5.7	97.68	356.39	0.01	0.4	0.00	0.37	37
Molise, Italy	CHT270	10/31/2002	5.7	97.68	356.39	0.01	0.5	0.00	0.41	35
CA/Baja Border Area	E11090	2/22/2002	5.31	52.3	196.25	0.12	2.9	0.06	0.31	22
CA/Baja Border Area	E11360	2/22/2002	5.31	52.3	196.25	0.13	3.5	0.07	0.30	21
Chi-Chi, Taiwan	CHY012N	9/20/1999	21:36	102.7	198.4	0.02	1.0	0.01	0.47	35
Chi-Chi, Taiwan	CHY012W	9/20/1999	21:36	102.7	198.4	0.01	0.8	0.01	0.47	43
Chalfant Valley	ZAK270	7/21/1986	6.19	7.58	316.19	0.45	36.8	1.94	0.48	6
Chalfant Valley	ZAK360	7/21/1986	6.19	7.58	316.19	0.40	44.7	2.00	0.60	8
Irpinia, Italy	BIS000	11/23/1980	6.2	14.74	496.46	0.06	11.9	0.10	1.07	21
Irpinia, Italy	BIS270	11/23/1980	6.2	14.74	496.46	0.07	12.2	0.09	1.26	22
Umbria Marche, Italy	NCR000	10/6/1997	5.3	9.33	428	0.45	14.5	0.67	0.19	5
Umbria Marche, Italy	NCR270	10/6/1997	5.3	9.33	428	0.29	11.8	0.59	0.19	4
Duzce, Turkey	DHM180	11/12/1999	7.14	178	354.37	0.02	5.1	0.02	1.55	26

Earthquake Name	Motions	Date	Magnitude (M _w)	R _{closest} (km)	V _{s30} (m/sec)	PGA (g)	PGV (cm/sec)	I _a (m/s)	T _m (sec)	D5-95 (sec)
Duzce, Turkey	DHM090	11/12/1999	7.14	178	354.37	0.02	4.6	0.02	1.38	26
Christchurch, New Zealand	CACSN40E	2/21/2011	6.2	14.41	280.26	0.18	17.2	0.32	0.40	13
Christchurch, New Zealand	CACSN50W	2/21/2011	6.2	14.41	280.26	0.23	20.3	0.48	0.56	10
CA/Baja Border Area	E07090	2/22/2002	5.31	56.96	210.51	0.08	3.9	0.04	0.33	32
CA/Baja Border Area	E07360	2/22/2002	5.31	56.96	210.51	0.06	3.4	0.04	0.40	42

Vita

Alisha Khanal was born in Chitwan, Nepal. She was the second child to Madhav Prasad Khanal and Sarmila Khanal. On June 2015, she graduated from Brindavan college of Engineering, VTU in Bangalore, India with Bachelor's in civil engineering degree. In August 2017, she joined the graduate program for civil engineering at The University of Texas at Tyler.

This thesis was typed by Alisha Khanal.